The long-range attraction between hydrophobic macroscopic surfaces

Patrick Kékicheff

The long-range attraction between hydrophobic macroscopic surfaces

Patrick Kékicheff

Université de Strasbourg, C.N.R.S. Institut Charles Sadron
23 rue du Loess, 67034 Strasbourg Cedex 2, France

email address: patrick.kekicheff@ics-cnrs.unistra.fr

Manuscript submitted to *Advances in Colloid and Interface Science*

Abstract:

Direct measurements of the long-range strongly attractive force observed between macroscopic hydrophobic surfaces across aqueous solutions are reexamined in light of recent experiments and theoretical developments. The focus is on systems in the absence of submicroscopic bubbles (preexistent or induced) to avoid capillary bridging forces. Other possible interferences to the measurements are also eliminated. The force-distance profiles are obtained directly (no contributions from electrical double layer or hydrodynamics) between symmetric identical hydrophobic surfaces, overall charge-neutral, at the thermodynamic equilibrium and in a quenched state. Therefore in the well-defined geometry of crossed-cylinders, sphere-flat, or sphere-sphere, there is no additional interaction to be considered except the ever-present dispersion forces, negligible at large separations. For the three main categories of substrates rendered hydrophobic, namely surfaces obtained with surfactant monolayers physically adsorbed from solution to deposited ones, and substrates coated with a hydrophobizing agent bonded chemically onto the surface, the interaction energy scales as $A\exp(-2\kappa D)/2\kappa D$ at large separations, with measured decay lengths in accord with theoretical predictions, simply being half the Debye screening length, $\kappa^{-1}/2$, at least in non vanishing electrolyte. Taken together with the prefactor A scaling as the ionic strength, the interaction energy is demonstrated to have an electrostatic origin in all the systems. Thanks to our recent SFAX coupling force measurements with x-ray solution scattering under controlled nano-confinement, the microstructuration of the adsorbed film emerges as an essential feature in the molecular mechanism for explaining the observed attraction of larger magnitude than dispersion forces. The adsorption of pairs of positive and negative ions on small islands along the interface, the fluctuation of the surface charge density around a zero mean-value with desorption into or adsorption from the electrolyte solution, the correlations in the local surface ion concentrations along the surfaces, the redistribution of counterions upon intersurface variation, all contribute and are tuned finely by the inhomogeneities and defects present in the hydrophobic layers. It appears that the magnitude of the interacting energy can be described by a single master curve encompassing all the systems.

1 - Introduction

Attractive hydrophobic forces play an important role in nature and industrial technological processes.[1-3] Examples include self-assembly of micelles, vesicles, and membranes,[4-7] folding of proteins,[8] wetting phenomena,[9] microfluidic transport, emulsion flocculation, destabilization of aqueous colloidal suspensions in mineral froth flotation separation process[10,11] where one of the colliding partner is a coarser air bubble and the hydrophobic particle will attach onto the bubble resulting in heterocoagulation. The hydrophobic force results from the underlying unfavorable solvation free energy of nonpolar solutes in aqueous or polar solutions. This so-called hydrophobic effect[4] manifests itself in many ways at the nano, meso, and macroscopic scales: hydrophobic moieties aggregate or cluster, oil separate from water, phase separation occurs, apolar/polar interfaces build up and arrange to create a large variety of structures (lyotropic liquid crystals), hydrophobic surfaces adhere strongly, water films dewet hydrophobic substrates resulting in a droplet with a large contact angle, etc. It was evidenced 50 years ago that two macroscopic hydrophobic surfaces may interact over large separations.[12,13] Since then, despite an extensive investigation, the experimental body of work on the range and magnitude of the hydrophobic force does not converge: recent overviews[14-17] summarize the measurements of the hydrophobic force between a large variety of substrates, the effect of solution conditions (Temperature, salt addition, gas dissolution…), and some of the artifacts that may have occurred. Even when these artifacts are circumvented, it has been concluded that the experimental results are themselves often contradictory. As pointed out by all the reviews the discrepancies are attributed to the fact that different experimental force-distance measuring techniques and different methods of hydrophobization result in different measured range and magnitude of the interaction, highlighting possible interferences to the measurements.[14-17]

The hydrophobic surfaces that have been employed to investigate the hydrophobic attraction experimentally can be classified into three main categories: (i) inherently hydrophobic surfaces such as bulk polymer surfaces; (ii) substrates coated with a hydrophobizing agent bonded chemically onto the surface; (iii) surfaces obtained with surfactant monolayers physically adsorbed from solution to deposited ones.

Among the inherently hydrophobic substrates (system i), solid polymer surfaces and soft hydrophobic systems such as oil drops in water and gas bubbles have been investigated. With any aqueous solution, an interface invariably carries or develops a surface charge.[1,2,18] This gives rise to an electrostatic repulsion due to the overlap of electrical double layers at such surfaces, explaining why, for instance, aqueous dispersions of polytetrafluoroethylene (PTFE, Teflon) particles[19] may remain stable despite the particles being hydrophobic. In aqueous solutions an electrical double layer repulsion also operates between oil droplets[20] and between gas bubbles.[21] The deformable interfaces of the soft hydrophobic systems add to the complexity of the overall interaction: as recently elegantly demonstrated, the local properties of the bubble surface vary during its interaction with another surface, and there is dynamic coupling between thin film flow and double-layer structure.[22] Therefore, inferring what are the strength and the distance dependence of the intrinsic hydrophobic attraction in soft hydrophobic systems is not an easy task despite efforts for suppressing as far as possible all the other interactions that contribute to the overall interaction.[17,20] Similar difficulties are met when the interaction between solid polymer surfaces is investigated. The development of surface charge leads to a double-layer electric repulsion that masks the attractive hydrophobic contribution as shown for polydimethylsiloxane films[23] and polystyrene surfaces.[24] In addition, solid polymer substrates usually present interfaces that are not atomically smooth, with a variation in the physicochemical and structural surface properties. Both the physical heterogeneity (above all roughness) of the solid surfaces and their chemical heterogeneity

have consequences not only for the range and magnitude of the attraction, but also for its variation with distance. The force-distance profile depends not only on solution conditions, but also on the history of previous contacts between the surfaces.[25] The appearance of step discontinuities in the profiles suggests that submicroscopic bubbles or cavities can be formed as soon as opposite surfaces had come into contact. These nanoscopic bubbles, which usually take place in roughness cavities, can coalesce and form gas bridges at the approach of surfaces. The formation of nanobubbles on solid surfaces requires a minimum of hydrophobicity as well as roughness and increases with further increase of the hydrophobicity, roughness, physical and chemical heterogeneities. Thus, when present, the long-range attraction between polymer surfaces (such as polystyrene[25-27] and teflon[28,29]) is usually consistent with a gas bridging (nanobubble) mechanism as observed in many systems of the second class (ii).

Indeed, for surfaces coated with a hydrophobizing agent bonded chemically onto the surface (such as silica surfaces coated with silane coupling reagents[30-38]), the origin of the forces measured for system (ii) has achieved the widest consensus. These chemisorbed hydrophobic substrates usually give a very high surface contact angle. On such surfaces, very small bubbles can attach stably when the substrates are in contact with an aqueous solution due to the incompatibility between the apolar surface and the polar medium. As suggested in the mid-1990s,[32] these nanobubbles coalesce and form a gas bridge when two opposite hydrophobic substrates approach close to each other, inducing a discontinuous attraction profile with the separation. The existence of cap-shaped nanobubbles was experimentally confirmed later by atomic force microscopy (AFM);[39,40] it has also been noted that large pancakes can form sometimes with large lateral expansion over several hundreds of nanometers and a height of a few nanometers.[41,42] What is attractive about bridging bubbles or cavities for these long-ranged forces is that the range of the force is related to their physical size. However, one conceptual difficulty with the small bubbles proposal is that, one would expect a lifetime of the order of microseconds, due to the high Laplace pressure inside the nanobubbles that drives the gas into the liquid. Since the pioneering works, the last two decades have seen a wealth of research on the nanobubbles and the resulting capillary force. A large focus has been on the direct imaging of nanobubbles using AFM and in-depth discussions to explain the existence and stability (> hours) of the surface nanobubbles (for recent reviews see refs. 43,44). It is now clear that in nearly all the systems (ii), what was thought to be a hydrophobic force was actually a capillary force resulting from the gaseous bridge formed from the coalescence of nanobubbles at the liquid-hydrophobic interface.[14,45] Thus, the so-called “hydrophobic” force measured in such cases appears to be a misleading term.[14,43,45]

On the other hand, it has been suggested that the origin of the force is different for the surfaces with physically adsorbed surfactants. Understanding the behavior in this third class (iii) of systems is also important for industrial applications and processes, ranging from detergency, dispersants or stabilization of suspensions,[46] paint and coating technology, surface conditioning (hair care formulations, sunscreens, make-up products, fabrics, dyeing, etc.),[47] filtration,[48] nanoparticle synthesis,[49,50] lubrication[51] to ore flotation[11]. The way the surfactant molecules interact with the substrate whether due to electrostatic attraction, hydrogen or covalent bonding, or hydrophobic forces, will determine the structure and morphology of the adsorbed film, and thereby how the surface properties of the substrate are modified when it gets coated. At a hydrophilic surface surfactant adsorption is highly cooperative and is in the form of surface aggregates (hemimicelles, admicelles, monolayered-like and bilayered-like patches).[46] For ionic surfactants adsorbed onto oppositely charged substrates, the cooperative nature of the adsorption is reinforced by electrostatic attraction. Determining the force-distance profile between two opposite surfaces with adsorbed

surfactants is of importance. It so happened the first indications of a hydrophobic attraction profile with separation were obtained with mica surfaces (negatively charged in water[52-54]) immersed in solutions of oppositely charged surfactant — the cationic cetyltrimethylammonium bromide C_{16}TAB.[55] Since then there have been many published accounts of hydrophobic forces measured between adsorbed layers of cationic surfactants with mica and silica substrates (for a review, see ref. 15). However, accurate determination of the force law has been prevented by intrinsic difficulties in the techniques used. Among many, the main limitation is due to the fact that, in most cases, the net attraction has been inferred by subtraction from a measured force that is overall *repulsive* (due to either hydrodynamic or electrical double layers). This procedure leads to considerable uncertainty, not only in cases where the hydrophobic attraction is long-range, but also when it is short-range. Indeed, except a few investigations detailed below, most of the measurements of the force between hydrophobic surfaces have been carried out with charged surfaces (for reviews, see refs. 14-17). The repulsive double-layer interaction present in such cases has to be subtracted from the measured force. But the assumed electrostatic repulsion has been calculated within the DLVO theory,[56,57] a too simplified framework as it does not take into account, beyond many, the structure of the water liquid close to the surface and the correlations between the ions. Therefore the resulting attraction deduced when so many free parameters are chosen to fit experimental data using a theory, that is anyway, clearly inapplicable[58-71] has confused the literature. In particular, these limitations explain why the effect of dissolved electrolyte on the measured interaction have resulted in a number of observations that appear to be contradictory, as it was already pointed out 25 years ago[72] and repeatedly underlined since then.

Actually, for charged surfactants adsorbing to oppositely charged surfaces from solution, there is a limited range of concentration for which the surfactant-coated substrate is overall electrically neutral, as it was demonstrated for the cationic C_{16}TAB adsorbed on negatively charged substrates such as mica,[73] glass[74,75] and silica[75]. Close to the point-of-zero charge (around 1/100 cmc (critical micellar concentration), the exact value depends on the surface charge of the substrate and hence the pH), there appears a long-range attraction, which is much larger than any possible van der Waals force.[73] Outside these narrow concentrations ranges, the surfactant-coated substrates carry invariably a surface charge. This interference inhibits a pure appraisal of the hydrophobic interaction for extended surfaces that are no longer globally electrically neutral. Indeed, measuring a total force that appears attractive does not mean that there are no repulsive double-layer forces but only that the attractive component is stronger at all surface separations. Thus, caution must be taken with previous works being hampered by electrical neutrality and stability-related issues, particularly as surfaces which were stable were not necessarily electrically neutral. This remark also apply for substrates rendered hydrophobic by chemical adsorption: see for instance the measured interactions between silanated mica surfaces that are actually not charge neutral.[76,77]

Additional complexity arises also when the thermodynamic equilibrium has not been achieved. This is well illustrated for non quenched systems such as surfaces with physically adsorbed surfactants for which exists a possible variation of surfactant adsorption upon change in the surface separation. The ability of the molecules to move around on a dynamic time scale upon changes in the water gap thickness between the two confining surfactant-coated substrates induces an adsorption instability.[78,79] This is particularly exacerbated for surfactant layers weakly anchored as observed for mica surfaces covered by ethoxylated amine surfactant.[80] This driven adsorption instability is also favored when the surfactant coated-substrates are not at the thermodynamic adsorption equilibrium.[81] Note also that insufficient equilibration time for surfactant adsorption may create film morphometries at solid / liquid interfaces that are not representative of the structural organization at the

thermodynamic equilibrium.[82] It should be emphasized that the interplay between *inter*surface and *intra*surface energetics generally implies that the desorption of the charged surfactant species is collective and occurs at a rather well-defined surface separation[79] (as opposed to a gradual charge regulation process such as ordinary double-layer interactions[83]). This suggests that such a collective desorption will be more likely if the charged species form surface aggregates that will desorb as an entity.[80] Whatever the mechanism is, the importance of being at the thermodynamic equilibrium is fundamental: as pointed out by Pethica, unless adsorption equilibrium is ensured, the Derjaguin approximation[84] is strictly invalid, and the calculated work of approach may not give the free energy.[78] As a consequence any measured force – distance profile between such opposite substrates cannot be utilized to infer the hydrophobic interaction potential of extended surfaces.

Although the existence of a long-range attractive interaction between extended hydrophobic surfaces is by now well documented, the variety of results suggest strongly that there is no single mechanism that can account for the diversity of behavior observed with differently prepared hydrophobic surfaces. According to the range of the interaction measured the results can be classified into three main categories: (i) an attraction of variable strength and range, often discontinuous with discernible steps on approach; (ii) a strong and short-range attraction between very stable surfaces; (iii) a long-range attraction with exponential decay.[14-17] The forces of type (i) are now well interpreted as resulting from the presence of small bubbles on one or both surfaces. Whatever the stabilizing factor for their existence is (surface-active materials originating from the preparation of the hydrophobic substrate (such as in the silylation procedure); sub-microscopic cracks and defects in the surfaces providing sites where bubbles may lodge, etc.), the interaction is a capillary-like force induced by the gaseous bridge formed from the coalescence of these nanobubbles at the liquid-hydrophobic interface. Therefore this interaction is not the focus of our present work. We will also leave the case (ii) out of the scope of the present article. Indeed, there are insufficient data to give an accurate functional form of these strong attractive interactions of short-range observed typically for gap widths smaller than a dozen of nanometers. This limitation arises from the sensitivity to details of the surface morphology and chemistry. Thus the variability in factors such as roughness, the precise nature of the chemical groups involved (such as $–CH_2$ or $–CH_3$), orientational effects and non-equilibrium, was pointed out as playing a significant role.[15] Rather, in the present article, we will deal with the attraction at long-range that has been reported in a variety of systems. These include substrates rendered hydrophobic with surfactant monolayers physically adsorbed from solution to deposited ones (dip-coating, Langmuir-Blodgett films), and self-assembling monolayers (SAMs) chemically adsorbed on surfaces (such as silane films).

The very long range strongly attractive force observed between macroscopic hydrophobic surfaces in aqueous solution is intriguing. The discrepancy between the results appears puzzling and a number of questions remain unanswered. However, these forces have been measured up to surface separations of 100 nm with magnitude that are 1-2 orders larger than those predicted by continuum theory (dispersions forces from Lifshitz theory[85]). It is a debated issue whether this deviation from continuum behavior should be attributed to molecular properties of the liquid, of the surface, or to surface interactions. Several theoretical explanations have been attempted and will be discussed in § 4: ordering of the liquid layers adjacent to the surface,[86] anomalous polarization due to local enhancement of the permittivity,[87] local fluctuation of adsorbed charges,[88,89] in-plane polarized domains with lateral dipole interactions,[90] cavitation instability,[91,92] ionic exchange coupled with ion-ion correlations,[93-95] dynamic structure in the confined liquid with collective vibrational motions[96,97].

Before proceeding it is appropriate to summarize the scope of this article. We narrow our focus to the long-range attraction (even asymptotic) operating between a pair of hydrophobic macroscopic surfaces. We restrict our description to systems that meet the following six criteria: (i) The opposite extended surfaces interact through a *well-defined geometry* (crossed cylinders, sphere-plane, sphere-sphere) with a local radius of curvature (typically in the range from 0.01 to 20 mm) several orders of magnitude larger than the surface separation range (0 – 0.2 μm). (ii) *No submicroscopic bubbles* are present at the liquid-hydrophobic interface or are induced when the opposite surfaces have come into contact. (iii) The surfaces are made of *identical material*: not only the underlying solid substrates are strictly identical in terms of homogeneity, smoothness, and physicochemical properties (such as wetting), but also their hydrophobic coating (physically adsorbed surfactant monolayer-like, chemisorbed silanized film) is prepared and achieved by means of the same procedure. (iv) They are surface-stable entities in aqueous electrolyte solutions. Long-term durability is here understood twofold. First coating integrity must be achieved for effectiveness preventing the absence of damage or local structural modification (at all the spatial and time scales) by means of the investigating technique. This means that the morphometry of the hydrophobic film is *quenched*, at the thermodynamic equilibrium. Secondly, the substrate / film assembly must be mechanically stable overcoming the often encountered limitation of ultimate film delamination or detachment of some coated parts from the substrate immersed in liquids. (v) The hydrophobic surfaces are *electrically neutral* in aqueous electrolyte solutions and hence there is no electrical double layer interaction contributing to the measured surface forces. (vi) the attractive force-distance profile is obtained *directly* from the force measuring technique in a quasi-static manner or when the *hydrodynamic contribution is negligible*. Since it is not obscured by any other repulsive forces (electrostatic, hydrodynamic, presence of nanobubbles), the long-range attraction between extended hydrophobic surfaces is nothing else than the gross attractive profile measured directly. Only the ubiquitous dispersion interaction remains but it is negligible at large separations.

Three systems fulfilling all these six criteria have been selected in our presentation. Optimum conditions in the preparation of the hydrophobic substrates have been privileged. There were monolayers of single-chain cationic water soluble surfactants (cetyltrimethylammonium bromide, C_{16}TAB) adsorbed on mica or glass surface, monolayers of highly insoluble double-chained cationic surfactant (dioctadecylammonium acetate, DODA, with either the acetate (DODAA) or bromide (DODABr) counterions) deposited on mica by dip-coating or by Langmuir-Blodgett, and glass surfaces hydrophobized by silanization.

In terms of experimental techniques, we start by review the four main devices and methods that have been used for measuring the force-distance profiles in these systems. We give a brief summary of facts necessary for the appreciation of the different experiments. In particular we emphasize the advantages and the limitations of each procedure (§ 2). Then the experimental data obtained both by other groups and by us are presented for the three aforementioned systems (§ 3). The fact that the long-range attraction profile in aqueous solutions obeys the same law for so different systems suggests that a similar mechanism is at play. Taking advantage of the electrostatic mechanism proposed for electrically neutral hydrophobic surfaces immersed in aqueous surfactant solutions,[94,98] we generalize this interpretation for the other systems (§ 4): only the inhomogeneities along the interface need to be recognized.

2 – Materials and experimental methods

Materials

Details on the materials as well as on the film formation or film deposition can be found in the respective articles referred to. Sometimes additional comments are proving necessary in order to pinpoint experimental subtleties. These will be given as and when issues arise.

Force-distance profile measurements

Of the various methods that have been devised for measuring molecular interactions, the most direct employ macroscopic solid bodies or extended surfaces. In any method of direct measurement of surface forces between bodies, the experiment reduces to the measurement of two quantities, namely, the force of interaction between the two bodies and the width of the gap that separates them. Both attractive and repulsive forces can be measured from the deflection of a balance arm or sensitive spring (cantilever) by means of electronics, optics, or interferometric techniques (for a review, see Kékicheff in ref. 63, pp. 204-280). For all these devices and techniques (force balance or spring devices) the measurements are carried out keeping the chemical potential of both solvent and solute constant. Thus, four main devices and methods have been used for measuring the force-distance profile between a pair of two macroscopic hydrophobic surfaces immersed in aqueous solutions. Beyond a brief description of the techniques that can be found in detail elsewhere, the scope of this section is to review the advantages and limitations of each method and to compare their capabilities.

1 – Conventional force-measuring method using a Surface Force Apparatus:

To date, most of quantitative experimental data concerning the effective range, distance and magnitude dependence of the hydrophobic interaction have been obtained[14-17] with a Surface Force Apparatus (SFA)[99]. Two partly silvered mica sheets, freshly cleaved along crystallographic planes and smooth at the angström level, are glued, silvered side down, onto the surface of two glass cylinders (radius of curvature ≈ 2 cm), aligned at right angles, one mounted on a piezoelectric tube, the other on a double-cantilever spring of stiffness K. The silvered surfaces form an optical cavity into which white light is directed and the surface separation, D, is determined to within 0.2 nm by the wavelengths emerging (Fringes of Equal Chromatic Order (FECO)[100]). The force, F, is determined with a deflection limit of 50 nN from the deflection of the double-cantilever spring on which one of the surfaces is mounted. In conventional force-measuring methods, the forces in aqueous solutions are measured by a stepwise compression of the surfaces: at each separation, usually about 10 - 30 s are allowed for a steady fringe position to be obtained before the next compression is initiated. In this respect the force-distance profile is obtained in a quasi-static way. The results are plotted as F/R vs. D, where the measured values of the force are normalized by the mean radius of curvature R of the surfaces. For the separation range considered ($D \lesssim 1$ μm) the distance between the surfaces is equivalent to that between a sphere and a flat plate (since $D/R \lesssim 10^{-4}$ typically throughout an experiment). Therefore the measured profile between crossed-cylinders corresponds to that of the free energy E per unit area of two equivalent flat parallel surfaces according to the Derjaguin approximation: $E = F/(2\pi R)$.[84]

The SFA technique is unique in being able to directly and unambiguously measure the local radii of curvature of the interacting surfaces, R, the refractive index changes,[100,101] and — very and most importantly — determine the absolute distance between the two interacting surfaces, i.e., with a defined $D = 0$ for bare mica substrates when in contact. However, several limitations have been noted.

(i) Quite rightly the possibility of defining an absolute scale of surface separation is hampered for experiments in which the mica surfaces are rendered hydrophobic by film deposition using dip-coating or Langmuir-Blodgett procedures. Indeed, after the measurement of the contact position in an atmosphere of dry nitrogen to calibrate the thickness of the mica sheets glued silvered back onto the curved silica disks of the SFA, the surfaces are transferred from the apparatus into a sealed chamber or a Langmuir trough to add the assembly of the film coating the mica surfaces. Once the coated-mica film is achieved the surfaces are repositioned into the SFA chamber. The operation of removing and repositioning the silica disks with the coated mica back into the SFA yields an uncertainty of about 1 nm in the determination of the absolute separation.[102] Larger uncertainties may arise in situations where film heterogeneities are observed. These heterogeneities can be preexistent or induced by film instabilities developed by prolonged immersion of the surfaces in electrolyte solution or by alteration of the local structure after repeated mechanical contacts (see § 3-2).

(ii) The forces seen as a continuous deflection away from contact are limited by the onset of deformation of the surfaces (as the glue between the silver layer and silica support disk is compressed). Thus, if the smallest normalized force can be detected to within 0.002 mN/m (that is a free energy of about 0.3 μJ/m^2), the maximum reliable measurable force will depend on the mechanical compressibility of the entire system. Typically surface deformations occur for applied loads larger than 8-15 mN/m and F/R becomes meaningless.[103,104] Note also the strong deformation of the surfaces when the surfaces are brought into a strong adhesive contact: because the glue adhering the mica to the discs is rather compliant a flattened region forms (of diameters of the order of 100 μm) as observed in the FECO fringe pattern. Thus, a large error can be made in inferring the interfacial energy γ from the measured pull-off force $(F/R)_0$ required to separate the two contacting hydrophobic surfaces in aqueous solutions ($(F/R)_0$ can be as high as 400 mN/m).

(iii) This conventional deflection technique is not suitable for the measurement of strongly attractive surface interactions because of the mechanical instability which occurs when the slope of the attractive interaction exceeds the stiffness of the force measuring spring K (the minimum constant stiffness of the double-cantilever is typically 50 N/m). Only forces in regions where $|\partial(F/R)/\partial D| \leq K/R$ can be measured. In these measurements only parts of the force curves are directly accessible and the force vs. distance profile appears discontinuous without the possibility of measuring any data, with jumps from unstable to stable mechanical regimes. Use of stiffer cantilever springs will increase the range of stability, but only at the expense of sensitivity in measuring the force. Another way to overcome this restriction is by means of a spring with a tension that can be varied during the course of an experiment, as explained next:

2 – Gradient method (Static jump-in method):

Strongly attractive forces can be measured by using the gradient method[105] based on determining the separation at which the spring instability occurs (the jump-in position) and this is recorded along with the spring constant. At this point the gradient of the force law $\partial F/\partial D$ equals or slightly exceeds the spring constant and the surface jumps to the next stable position of the force curve. Provided that the thermal and mechanical drift of the surfaces is negligible, the spring constant divided by the mean radius of curvature of the hemi-cylinders K/R is assumed to equal $\partial(F/R)/\partial D$. The precision involved in these measurements is less than when measuring the force directly, particularly when the second derivative of the force is small. Typically at the onset of instability the accuracy in separation is about 0.5-1.0 nm. In the SFA a variable double-leaf spring is used to carry out measurements at different points along the attractive profile of the interaction.[105] This is accomplished by clamping the spring at different distances along its length by use of a rod that could be manipulated from outside

the liquid chamber. In this way the spring stiffness can be varied by more than a factor of thousand (from about 10^2 to 10^5 N/m) during an experiment providing the means for determining the slope of attractive forces over a large range of distances[105,106] Thus, in the gradient method a plot of the derivative of the force between the two crossed cylinders, which in the Derjaguin approximation is just the pressure between flats, P, can be constructed ($\partial(F/R)/\partial D = -2\pi P$) as a function of separation D where the surfaces begin to jump.

3 – Balance arm method:

To overcome the difficulty encountered in measuring attractive forces that increase drastically as the distance between the surfaces decreases, devices provided with negative feedback have been used. Negative feedback automatic control is a powerful arrangement, which accomplishes a quadrupole purpose: (i) it allows one to set the gap at any desired distance; (ii) it maintains the separation by producing a force equal and opposite to the interaction; (iii) through negative feedback it corrects any drift of the surfaces from the preset position; and (iv) it provides a means of measuring the opposing force. Thus the crossed-filament method was developed with success to investigate the surface forces between solids in gaseous and liquid media.[107-109] For the investigation of the long-range hydrophobic attraction, thin fused quartz wires (radius: 0.5–1.5 mm) hydrophobized by silanation and crossing at right angles were used.[30] In this set-up the movable thread serves as part of a photoelectronic follow-up system, which automatically ensures the stability of its position to an accuracy of up to a few tenths of a nanometer. Unlike a simple mechanical system, it is possible to vary the effective spring constant of the system by altering the gain in the feedback circuit. In other words, the capability exists to alter electronically the stiffness of the force measuring system. In this method the measured force is automatically counterbalanced by maintaining a preset gap width D between the surfaces even in the range of large values of $\partial(F/R)/\partial D$. The forces can be measured with great sensitivity to within 1 nN (that is a free energy of about 0.11 $\mu J/m^2$). Note also that the use of smaller sample sizes is of considerable advantage as the amount of steric hindrance due to the roughness of the surfaces is concomitantly reduced. The only drawback of this set-up consists of a certain inaccuracy in the determination of the contact position. In addition to the unevenness of the surfaces, the absolute scale in separation appears to be uncertain at about 1 nm.

4 – Dynamic force-measuring methods:

Another method that partly overcomes the spring instability problem and allows continual recording of both repulsive and attractive surface forces, is to drive the two surfaces toward each other with a constant driving speed. At very large separations they will approach one another with a uniform velocity, but at smaller separations the cantilever on which one of the surfaces is mounted will start to deflect as the surfaces begin to feel a force. This progressive deflection of the spring due to hydrodynamic and surface forces means that the surface itself does not move any longer at constant speed. In this method the distances are measured as a function of time and the force calculated from the equation of motion of the moving surface.[110] The surface force, supposed to be the "equilibrium" surface force, is inferred by subtracting a calculated hydrodynamic force from the measured total force. This procedure assumes that the relative velocity of the surfaces at all times is sufficiently low that equilibrium forces operate between the surfaces. Inertial and acceleration effects are also ignored. The inferred attractive force-distance profile suffers from the complication that the viscosity of the liquid medium must be known accurately and for thin films there is no guarantee that is should equal to the bulk value. An additional complication is the assignment of the slipping boundary (the shear plane) to calculate the hydrodynamic contribution to the total force. No-slip boundary condition has often been assumed, and even when significant

slip lengths (tens of nanometers) should be more appropriate for describing the flow of water in the vicinity of a hydrophobic-water interface.[111,112] Furthermore elastohydrodynamic effects, which may deform the surfaces due to a nonuniform pressure between them, cannot safely be ignored. To conclude, the attractive profiles obtained between hydrophobic extended surfaces using the dynamic drainage method by means of the SFA must be critically re-examined when so many assumptions are at play. The presentation of these results is postponed in a forthcoming article.

Nevertheless the use of smaller sample sizes ($\lesssim 2$ mm) allows the hydrodynamic contribution of aqueous solutions to be rendered negligible since the latter scales with the square of the radius.[110] This is of considerable advantage as many of the aforementioned assumptions are no longer required. Two main geometries have been considered for measuring the attraction between hydrophobic extended surfaces: the sphere-plane and the sphere-sphere geometries.

In the colloidal probe technique, developed in 1991 independently by Ducker *et al.* [113] and by Butt[114], a colloidal particle of few micrometers in diameter is attached to the microfabricated cantilever of a standard Atomic Force Microscope (AFM). A micromanipulator allows the particle to be glued at the end of the (tip-less) cantilever (100–200 μm in length). As the AFM scanner is lifted toward the probe the deflection of the cantilever is monitored by means of the light-lever method, in which the laser beam reflected from the back of the cantilever is detected with a split photodiode.[115] The force measured through the deflection of the cantilever is recorded as a function of the vertical displacement of the AFM scanner positioned with a precision better than 0.1 nm. A force resolution of 10–50 pN can be achieved, and by subsequent averaging of the force profiles, the noise can be reduced by one order of magnitude at least. Another advantage of the technique lies in a well-controlled geometry of the interaction, as the ill-defined radius of curvature of the sharp AFM-tip on the cantilever is replaced by a spherical particle with known (or easily measurable) surface radii. With particle radius in the range 1-100 μm, the free energy of the interaction between the sphere and the flat can be measured to within 0.02 $\mu J/m^2$. While the relative surface separation can be determined with a resolution of 0.1 nm or better, the absolute surface separation is obtained from the onset of the constant compliance region. This onset can be determined for solid samples with a precision between 0.5–2 nm; however, its location becomes problematic for soft repulsive interactions and for deformable surfaces. Actually, the whole technique essentially hinges on the interpretation of that region when the two surfaces come together and their motions become mechanically coupled. Several difficulties arise. In this region it is assumed that the surfaces are incompressible, and consequently only the cantilever is deformed under the loads applied. For some systems, especially those where the surfaces have adsorbed species, for example ions and surfactant molecules, higher applied loads may result in a change in the surface separation or in the slope. This is a result of either the forced desorption, compression, or depletion of species and subsequently another region of constant compliance may be attained. Whether or not an adsorbate can be displaced will depend upon the probe radius, as it is the applied pressure that is important. As a consequence not only the magnitude of the force may be in error (since it is transformed via the slope of the compliance regime) but also the separation. Since distances are calculated relative to a hard wall contact, the method does not allow an absolute scale in separations to be set.

The classical colloidal probe technique measures forces between a spherical particle and a planar substrate, and therefore such a system is inherently *asymmetric* as one usually cannot guarantee identical materials for the spherical probe particle and the planar substrate, except in very rare cases reported in the literature where this precaution was taken.[94] Asymmetry artifacts can be eliminated by measuring forces between two identical particles.

As recently discussed this sphere-sphere geometry requires a lateral alignment of the two particles within the AFM.[116]

In the MASIF (Measurement and Analysis of Surface Interaction Forces)[117,118] both the sphere-plane and the sphere-sphere geometry can be used. Usually flame polished glass surfaces are used (radius ≈2 mm), prepared by melting the end of a glass rod in a butane-oxygen burner. The surface energy of the glass causes the molten glass to form a highly smooth (RMS roughness of 0.2 nm) spherical drop on the molten end. One of the surfaces is mounted on a bimorph sensor while the other one is made to approach using a piezoelectric crystal. An experiment is conducted and analyzed in much the same way as with an AFM when used for force measurements. The surfaces are brought together into contact in a continuous manner, and then separated apart. When the surfaces meet a "hard wall" contact, the motion of the ramping moving surface is directly transmitted to the bimorph allowing the sensitivity of the force sensor to be calibrated (this assumes of course that the surfaces are incompressible). Thus the deflection of the bimorph is known at each instant within 0.05 nm, and the force exerted is obtained using Hooke's law and the spring constant (accurately measured from the resonant frequency of the device; in the range 100–500 N/m). Assuming that the local radius R at the interaction point does not differ significantly from the macroscopic radius, the resolution in normalized force F/R is about 0.01 mN/m (that is a free energy of about 2 $\mu J/m^2$ since for two interacting spheres, the factor is π differing by a factor 2; see eqn.2). As the surface separation is calculated from the known expansion of the piezoelectric tube and the measured bimorph deflection, the reported distance in the force profiles is relative to the position of the hard wall reached in each force run.

In conclusion, all techniques provide a good spatial resolution on the order of 0.1 nm or better, but they do not necessarily give the *real* separation between the surfaces. Indeed, surface deformations may occur prior to the surfaces contacting each other: the effect of a repulsive surface interaction is to flatten the surfaces and to increase their separation compared to the undeformed surface shape, whereas the surfaces bulge out toward one another under the influence of attractive forces. These deformations may become significant at short separations (a few nanometers), amounting to the same order of magnitude than the gap width. Only the interferometric SFA gives a direct access to the *real* separation between the surfaces, whenever they are deformed or not. In all the other techniques the separation extracted is the distance between surfaces, as *if* they were not deformed. And even in the case when no deformation occurs, the technique of driving continuously one surface toward the other one until they come into contact suffers from a main deficiency, which ultimately restricts the use of the colloidal probe AFM and MASIF force measurements, namely the impossibility of defining an *absolute* scale in surface separation, unlike the SFA. The resolution in the free energy lies in the 0.02 – 2 $\mu J/m^2$ range with the best resolution provided by means of the colloidal probe AFM technique. On the other hand, the upper limit depends on the most elastic component of the device and is usually governed by the means of attaching the surfaces (for instance the underlying glue fixing the mica sheet to the silica hemicylinder in the SFA or the microscopic sphere to the cantilever in the AFM). The inherent limitations of all these techniques are related to the fact that under high applied loads surface deformation becomes substantial and measured values of F/R no longer corresponds to the free energy of interaction as related by Derjaguin approximation. One can also note that AFM microfabricated cantilevers and MASIF bimorphs are both single leaf springs and hence will lead to an underestimate of the measured adhesion.[119] Indeed, upon separation the motion of the surfaces does not remain parallel and the surface that is mounted on the cantilever rolls and shears against the other, with a consequent substantial shift in the point (or area) of contact and a concomitant reduction in the pull-off force. By contrast, this drawback is

reduced with the use of a double cantilever spring (as in the SFA) because the motion of the spring-mounted surface is constrained to move parallel with the motion of the opposite surface. Furthermore, despite the fact that the hydrodynamic contribution may sometimes be rendered negligible in the devices where one surface is ramped continuously toward the opposite one (and apart), the measured dynamic (or instantaneous) force is still supposed to be the "equilibrium" surface force and this for every separation, as if there was no effect of the liquid drainage between the two approaching surfaces. This may be questionable for adsorbing ions and surfactant molecules that can exchange slowly with the bulk, particularly for systems that are not quenched and not at the thermodynamic equilibrium. Finally all the devices suffer from the same spring mechanical instabilities: only forces in regions where the gradient of the force is smaller than the spring constant can be measured, and the corresponding force-distance profiles appears discontinuous with inaccessible parts.

3 – Results

Now that we have reviewed and seen how the techniques work, let us present the force-distance profiles obtained for the three classes of systems.

3 – 1 – Physically adsorbed surfactant on substrates in equilibrium with aqueous surfactant solutions

Among physically adsorbing systems, that is, in systems where chemical interactions are absent and adsorption at low concentrations occurs through electrostatic interaction between the surface and surfactant ions charged oppositely to the surface, quaternary alkyl ammonium bromide surfactants C_nTAB (n = 6-20) solutions in contact with mica, silica, glass or quartz have given a wealth of data in the last three decades. Particularly, below the critical micellar concentration (cmc), the adsorption on these substrates and the behavior of cetyltrimethylammonium bromide (C_{16}TAB) solutions in their vicinity have been characterized by many experimental techniques, including AFM imaging,[82,120-124] streaming potential,[125-128] neutron,[129-133] X-ray[134,135] and optical reflectometry,[125,136-138] X-ray photoelectron spectroscopy (XPS),[139,140] spectroscopic techniques (infrared,[141-144] fluorescence quenching,[145] Raman[144,146,147]) to NMR techniques (see refs. 148-150 and references therein), calorimetric and thermodynamics studies[151]. Theoretical modeling[152] and numerical simulation studies[153,154] have also shed some light into the physical behavior of these self-associating systems at the solid/liquid interface. In terms of direct force measurements, different techniques have been used. These include the surface force apparatus (SFA),[55,73,101,106,155] the MASIF,[74,75] the AFM colloidal probe technique[94] (other works also reported force profiles between underlying asymmetric surfaces being not at the adsorption thermodynamic equilibrium[156,157]), and the SFA coupled with x-rays scattering (SFAX) [98].

As for any charged surfactants adsorbing to oppositely charged surfaces, there is a limited range of concentration for which the surfactant-coated substrate is overall electrically neutral. On mica substrates immersed in increasing C_{16}TAB concentration aqueous surfactant solutions (pH ~ 5.7) the surface charge first decreases to become neutral at some concentration close to 4 x 10^{-6} M, after which there is a build-up of charge again.[73] On glass[74,75] and silica[74] the trends with increasing solution concentration of C_{16}TAB are similar. Nevertheless the isoelectric points for the surfactant-coated substrates occur at different bulk concentrations, because of the higher charge of the mica surface at normal pH (~5.7)[53] compared with silica[158,159]. For instance the isoelectric point for C_{16}TAB is at 4 x 10^{-5} M at pH 6.5 on quartz.[126] It is only at pH 10 that the C_{16}TAB-coated silica behavior mimics, not

only qualitatively but also quantitatively, the C_{16}TAB-coated mica behavior at pH 5.7. Thus at pH 10, the charge reversal of glass occurs in the 3–6 x 10^{-6} M range and a bilayer forms at about half the cmc,[75] exactly as was observed previously for mica at pH 5.7[73].

Close to the point-of-zero charge there appears a long-range attraction, which is much larger than any possible van der Waals force.[73] Between two electrically neutral surfactant-coated like-surfaces (such as mica or glass) attractive forces decaying exponentially at large separations with a measurable range up to about 100 nm have been found. The results of measurements suggest that the nature of both the surface and of the ions in solution has an effect of the range and magnitude of the hydrophobic attraction. More precisely at large separations D (i.e. $D \gg \kappa^{-1}$ with κ^{-1} the Debye screening length) its dependence on electrolyte concentration has been described as scaling as:[94]

$$\frac{F}{R} = -A\frac{\exp(-2\kappa D)}{2\kappa D} \tag{1}$$

Through use of the Derjaguin approximation,[84] the force normalized by the local radius of curvature of the surfaces, F/R, may be related to the free energy interaction per unit area between two parallel, flat surfaces, E:

$$\frac{F_{\mathrm{cc}}}{2\pi R} = \frac{F_{\mathrm{sf}}}{2\pi R} = \frac{F_{\mathrm{ss}}}{\pi R} = E \tag{2}$$

where the subscript cc stands for crossed cylinders, sf for a sphere against a flat, and ss for two spheres. The pseudo-exponential law can be expressed as:[94]

$$E = -\alpha k_B T L_B \rho_{\mathrm{tot}} \frac{\exp(-2\kappa D)}{2\kappa D} \tag{3}$$

where ρ_{tot} is the total ionic density, $L_B = e^2/4\pi\varepsilon_0\varepsilon_r k_B T$ the Bjerrum length of the solvent (≈0.7 nm at 25 °C for water). Both the pseudo-exponential behavior and the dependence of the prefactor upon the ionic strength suggest an electrostatic mechanism. Twenty years ago we already interpreted this long-range attraction between similar, charge-neutral surfaces as resulting from the coupling between the two opposite substrates via charge fluctuations due to the adsorption of pairs of positive and negative ions on islands of inhomogeneities along the surfaces.[94] In our proposal, walls appear inhomogeneous provided the islands of inhomogeneities are sufficiently far apart along the interface. Typically two adjacent islands must be separated by distances larger than the wall separation; otherwise their contribution to the attractive interaction will be reduced by electrostatic correlations along the plane.[93,94]

To shed some light into the role of the inhomogeneities along the interfaces recognized as the governing source of the observed long-range attraction,[94] we measured the surfactant-surfactant correlations by an *in situ* scattering technique as a function of the confinement gap. Taking advantage of the sub-nanometer resolution in surface separation accessible provided by a Surface Force Apparatus, we purposely designed a setup coupling the SFA technique with x-ray scattering. Our advanced device, named SFAX,[98] with enhanced spatial and time resolution and automation was specifically built for the SIRIUS beamline[160] at the synchrotron radiation facility SOLEIL, France. It allows the relationship between force, distance and structure to be sought under controlled nano-confinement and stress. Here the coupling of the two techniques (X-ray and SFA) has been envisaged in the transmission geometry where the incident x-ray beam is impinged normally to the two

confining surfaces. In this configuration scattering vectors Q parallel to the mica surfaces are obtained and the 2D-detector collects the photons transmitted through the sample. Thus the equatorial plane of the reciprocal space is described and the SFAX measures the lateral structural information along the surfaces whose separation can be varied continuously under controlled nano-confinement with a sensitivity of 0.2 nm.[98]

Note that the x-ray scattering originates from the *same* volume of the confined sample under stress, that is from the *precise* local spot where the force-distance profile is measured. To satisfy this requirement, a careful alignment of the SFAX with the x-ray incident beam axis has been sought. To fulfill this goal, several technical necessities have been solved: (i) *a precise alignment of the two horizontal axes of incidence:* the SIRIUS goniometre platform is moved to make the SFA optical axis to coincide with the SIRIUS beamline by aligning the center of the Newton rings (viewed when the two back-silvered mica curved surfaces are shined by monochromatic light) with the incident x-ray axis. (ii) *a volume of the irradiated sample as small as possible:* since the surface forces measured in the SFA correspond to the liquid mediated interactions between the two opposite immersed surfaces over a ≈50 µm cross-section area (see ref. 63, pp. 204-280), the incident x-ray beam is collimated with a cross-section ≤ 50 µm. Otherwise, insufficiently collimated beam would obscure any quantitative measurements: see the drawbacks obtained with a 125 µm x-ray beam at Stanford Synchrotron Radiation Laboratory with the first SFAX coupling attempts[161,162] for which the scattering is convoluted and averaged through several structural configurations in the confined space of continuously varying thickness due to the curvature of the surfaces (radius ≈2 cm). (iii) *an optimization of the scattered signal:* to obtain a good transmission and avoid unwanted diffuse, diffracted, specular signal from the supporting holders, the incident and scattered x-rays must cross the confining mica surfaces *only*. To achieve this requirement for mica immersed in a liquid environment hollow glass hemicylinders with centered small rectangular apertures (4 mm long along the summit ridge axis; 1.5 mm wide) were designed. The back-silvered atomically smooth thin mica sheets (≈5 µm) seal the apertures. Thus, the micas placed at the entry and exit insure not only the sealing of the hemicylinder apertures but also allow an enhanced transmission as the x-ray path is considerably reduced since the emerging photons scattered by the confined sample no longer cross any additional bulk sample (Fig. 1).

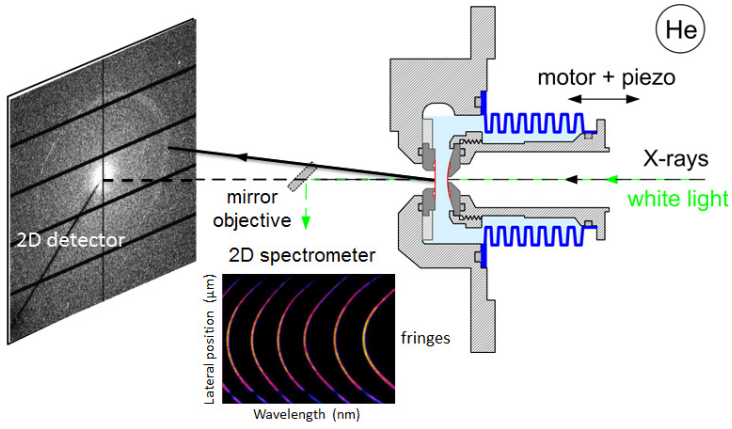

Figure 1: Coupling the Surface Force Apparatus with X-ray scattering: General principle of the SFAX[98]

The incident x-rays fall at normal incidence on two atomically smooth mica surfaces (thickness ≈5 µm; radius of curvature ≈2 cm) freely suspended from the SFAX, allowing the equatorial plane of the reciprocal space to be described. By bringing the movable upstream mica surface closer to or further away from the fixed exit mica surface, the separation is varied, checked at every step, and measured to

±0.2 nm using white light interferometry with a set of mirrors and retractable objectives for in-situ coupling with the x-rays. Taking advantage of the surfaces position stability (drift < 1 nm per minute[63,102]), the incident x-rays are thus allowed to cross the mica surfaces and irradiate the confined sample at the same location exactly: the scattering pattern is collected on the 2D PILATUS3 (Dectris Ltd, Switzerland) detector of the SIRIUS beamline[160] at the SOLEIL synchrotron radiation facility, France. The successive measurements set by the two techniques are repeated at each position of the upstream surface. The confinement gap is varied in a continuous and controlled manner at a sub-nanometric scale by means of a piezo element superimposed on the coarse positioning range of a motorized micropositioner. Thus, the structure is determined as a function of the surface separation (from tens of micrometers down to mechanical contact) under controlled nano-confinement. The SFAX is placed in an enclosure, from the Beryllium window at the beamline exit to the PILATUS detector at a ~4.5 m distance from the SFAX, filled with Helium to avoid spurious scattering by air and also oxidation of the 50 nm thick silver layer coating the back of the mica sheets and its degradation under high incident flux of x-rays.

As the x-rays cross the freely suspended mica curved surfaces at exactly their contact point, the determined structural information corresponds to the measured interactions between the two opposite immersed surfaces. Taking advantage of the well established experimental situation of negatively surfaces in aqueous solutions rendered electrically neutral by immersion in the C_{16}TAB cationic surfactant solutions,[73,94] the mica surfaces of the SFAX were incubated in a ≈1/120 cmc C_{16}TAB solution at 25 °C above the Krafft boundary and for 24 h to ensure that the thermodynamic equilibrium is reached[73,82] at such low concentrations well below the critical micellar concentration (cmc ≈0.9 mM at 25°C [163,164]) in water. Figure 2 presents the evolution of the scattering pattern collected at small angles as a function of the confinement gap. A weak diffuse scattering ring whose scattering vectors are parallel to the surfactant-coated mica surfaces is revealed in the equatorial plane.[98] When the surface separation D is large enough, the magnitude and the position at $Q_{\parallel} \approx 0.054$ Å^{-1} of this diffuse ring almost do not evolve as well as the overall scattering pattern (Fig. 2). Conversely, the intensity and the shape (to a lesser extent) of the latter are affected as soon as $D \leq \xi^* = 2\pi/Q_{\parallel}^* \approx 12$ nm. These evolutions suggest a subtle interplay between the characteristic length set by the microstructure and the gap width — the correlation length ξ along the planes and the separation D along the normal direction — with a remarkable crossover occurring at $D \sim \xi^*$. When passing from large to small separations in the confinement gap the intensity increases almost stepwise at separation ξ^* by about 80%; it is followed by a smoother evolution upon further reduction of the surface separation. The position of the diffuse scattering bump observed in the equatorial plane suggests a lateral correlation length $\xi^* \approx 12$ nm along the hydrophobic substrate. The absence of second order underlines that there is no order propagation at long range; its width would correspond to a domain size (correlation length) of ≈50 nm.

The magnitude enhancement of the diffuse scattering as soon as the spatial crossover is attained can be understood simply with the following paradigm. When the separation between the two opposite-like surfaces of the SFAX is large (for $D \gg \xi^*$), the in-plane layer scattering produced by one wall is similar to the other one as they behave independently (both provide equal scattered amplitudes: $A_1(Q) = A_2(Q)$). As a result the collected scattering pattern is $I(Q) = \left(A_1(Q) + A_2(Q)\right)^2 = 4I_1(Q)$ independent of the confinement gap D. Conversely when the separation D along the normal direction decreases and becomes of the order of ξ^*, the crossed-term in the former equation is no longer negligible and $I(Q) = \left(A'_1(Q) + A'_2(Q)\right)^2 = 2I'_1(Q) + 2A'_1(Q)A'^*_2(Q)$ for $D \leq \xi^*$. The fact that both the position and the shape of the diffuse bump are not greatly affected when the crossover $D \sim \xi^*$ is passed in either direction (behavior fully reversible) suggests a slight or slow structural

rearrangement of the adsorbed hydrophobic layers, provided they have not come into contact. Indeed, a mechanical contact of the two opposite C_{16}TAB-coated surfaces induces cavitation[73] and irreversible structural changes (data not shown). The (almost stepwise) intensity enhancement of the overall diffuse scattering as soon as the spatial crossover is attained matches our expectation for *quenched* patterns.

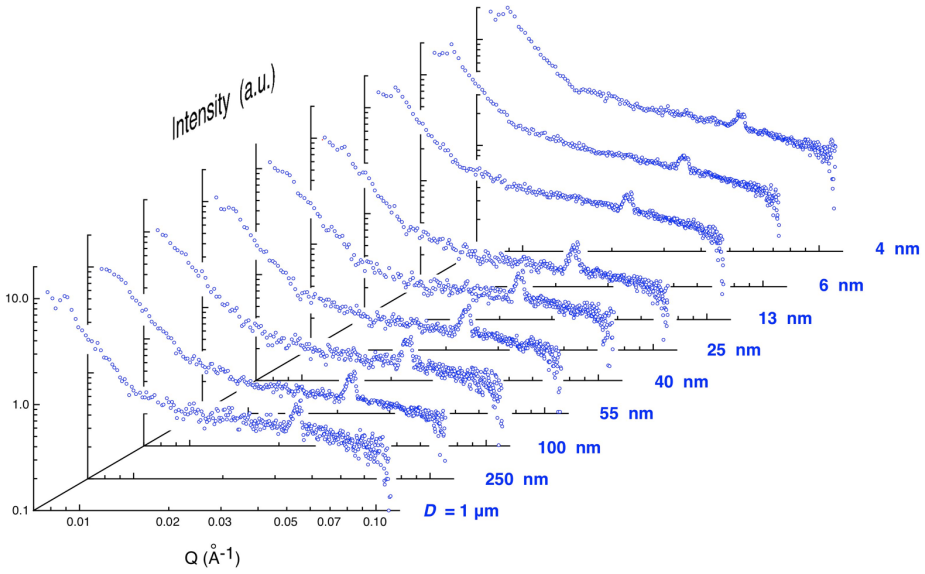

Figure 2: Scattering curves for different separations between mica surfaces immersed in an aqueous C_{16}TAB solution at ≈1/120 cmc (24 h equilibration; 25 °C) observed in the geometry of Fig.1. The log-log scale highlights the different regimes encountered for the variation of the scattered intensity with Q. At large surface separations, D, the scattering curves are all similar with almost no variation in position, shape and magnitude of the bump at $Q_{\parallel}^{*} \approx 0.054$ Å^{-1}. Conversely a uniform stepwise increase by a factor 1.8 in magnitude occurs as soon as D decreases below 13 nm. This transition is nearly reversible whenever the confinement gap is reduced below this threshold or increased beyond. All the radial averaging data have been corrected for the scattering contribution of the mica sheets immersed in pure water using standard subtraction procedures.

Indeed, in the narrow concentration regime of charge inversion and after long equilibration the adsorbed C_{16}TAB molecules have ultimately built patchy patterns composed of connected monolayer-like stripes (mica surface coverage ≈2/3).[82] As we noted, the interaction of the cationic surfactant with the opposite negatively charged mica surface is determined primarily by the head groups. The concomitant rearrangement of the hydration regions leads to stronger bonds and increases the kinetic barrier to desorption. Coupled with the hydrophobic interaction between the alkyl chains of neighboring surfactant molecules, the ultimate adsorbed aggregates get a cohesive energy sufficiently large to make any desorption process less favorable, since it would imply a collective process. Thus at the thermodynamic equilibrium, the adsorbed film composed of alternating bare and covered patches without any long-range order behaves as a *quenched* system as we have recently shown.[82] When the separation between two opposite C_{16}TAB-coated mica surfaces is varied the quenched micro-structuration of the adsorbed surfactant layers makes arrangements of bare/covered areas by surfactants to be too slow. However, counterions (potassium ions dissociated from mica, and bromide ions from C_{16}TAB) can respond by redistribution in the confinement gap. This occurs when the structures on opposing surfaces start to interact. When agonistic patches happen to face the bare mica areas and the monolayer stripes both attract excess counterions. Conversely for facing antagonistic patches (bare mica vs. monolayer) their excess counterions (Br^- and half of the K^+) are released and leave as neutral salt.

As discussed previously,[98] since the counterions dominate the scattering their (local) release/increase merely amounts to a new x-ray labeling of the pattern with the contrast (almost stepwise) increasing upon approach of the surfaces. In this quenched case the dominant effect is an almost homogeneous variation of the scattered intensity with superimposed minor deformation and almost no displacement of the scattering peak. The variation of the scattering pattern upon confinement confirms the dominating mechanism of local counterion release/increase suggested earlier for explaining the long-range electrostatic attraction between similar, overall charge neutral walls.[94] It also emphasizes the role of the inhomogeneities along the interfaces as the main source for a long-range electrostatic attraction to occur (see also § 4).

To encourage consistency and strengthen the description by a generalization to other substrates in different solution conditions, we start by further monitoring the effect of the surface charge density of the underlying supporting substrate. Figures 3 and 4 show the force-distance profiles measured by Parker *et al.* for the same cationic C_{16}TAB surfactant adsorbed on glass.[74,75] In these works the MASIF technique was used with two identical glass spheres rendered hydrophobic and essentially non-charged by adsorption of the cationic surfactant at two different pHs. At normal pH (~5.6) the charge on glass is neutralized at 4–5 x 10^{-5} M [74] whereas at basic pH 10 this occurs at smaller concentrations (in the range 3–6 x 10^{-6} M)[75] since the silanol density of the silica interface in water is higher.[158,159] At these isoelectric points the measured interaction is purely attractive, with a reported magnitude much larger than the expected screened dispersion forces for silica surfaces across aqueous surfactant solutions, and comparable to those reported in literature. At long range the attraction appears to decay exponentially but at smaller separations the attraction starts to increase more rapidly. We took advantage of the analysis proposed earlier[94] to take into account the enhanced attraction by scaling the measured interaction as $\exp(-2\kappa D)/D$. A combination with the expected screened dispersion forces has a negligible effect on the numerical fit to these experimental data. Indeed, at short separations, due to a small value of the Hamaker constant ($H \sim 8 \times 10^{-21}$ J) the nonretarded van der Waals attraction ($F_{\mathrm{vdW}}/R = -H/6D^2$) contributes little to the total interaction. At large separations the effect of retardation and screening by an electrolyte has been calculated within the framework of the Lishitz theory[85,165] using the useful Ninham-Parsegian representation for the dielectric susceptibilities of the media[166,167] with the complete representation for water as given in ref. 53. Our calculations (not presented in this manuscript) do not change the quantitative conclusions of the aforementioned analysis. Thus, in Figures 3 and 4 the solid lines represent forces calculated using eqn.1 under the assumption that it originates from the plane coinciding with the solid surface (bare glass). Over the almost whole range of separations, the numerical calculations describe the experimental data satisfactorily, despite their twofold limitations: a large scatter in the data (especially those that were measured at pH~5.6 [74] and reported in Fig.3) and the uncertainty in the absolute scale separation with its intrinsic ambiguity in the zero at contact (we recall that the MASIF technique cannot define the separation with respect to the contact between the two bare surfaces in dry atmosphere; see § 2). However beyond a general agreement with eqn.1, we note that at short separations the fits underestimate the forces somewhat. This deviation occurs when the confinement gap is reduced below a thickness of the order of κ^{-1}. This occurrence, already experimentally reported previously, is in agreement with the theoretical framework that lead to the establishment of eqn.1, emphasizing it is an asymptotic law only.[93,94] Except for this deviation at the shortest surface separations, the screening lengths extracted from the fits correspond to the expected Debye lengths at the corresponding ionic strengths of the surfactant solutions: asymptotically, the decay length of the attraction is simply $\kappa^{-1}/2$. Therefore it appears that the attractive force-distance profile is governed by one fitting parameter only: the prefactor A of eqn.1 giving its overall magnitude.

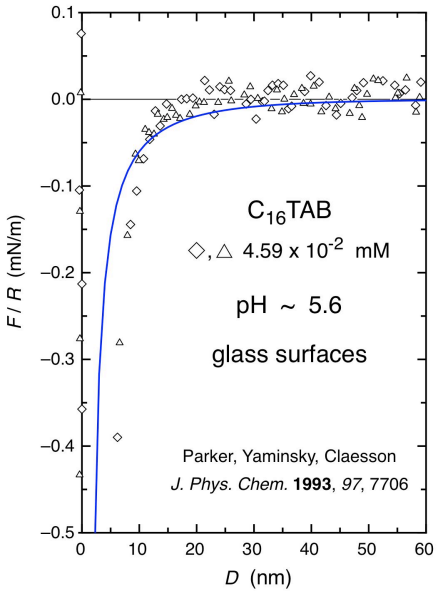

Figure 3: Surface forces between two glass spheres immersed in an aqueous solution of 4.59 x 10^{-5} M $C_{16}TAB$ at pH ~5.6.[74] The force F, normalized by the sphere radii R (~ 2 mm), is measured as a function of the (relative) surface separation D by the MASIF technique (the different symbols are those reported in the original data, Fig. 3 of ref. 74). The reported distance in the force profiles is relative to the position of the hard wall reached in each force curve. The solid line shows the interaction law given by eqn.1, $A\,e^{-2\kappa D}/(2\kappa D)$, and calculated with a screening length κ^{-1} = 42 nm and a prefactor A = 0.05 mN/m, under the assumption that it originates from the plane coinciding with the bare glass surface (adsorbed surfactant layer thickness ~1.5 nm on each sphere[74,75,94]). Given the scatter in the data and the ambiguity of the zero separation, an uncertainty of ± 3 nm has been estimated for κ^{-1} with A lying in the range 0.04 – 0.07 mN/m. The fitted parameters correspond well to the expected Debye length 43.7 nm at the ionic strength of the $C_{16}TAB$ solution, and to the expected prefactor of eqn.3 (see also Fig. 5).

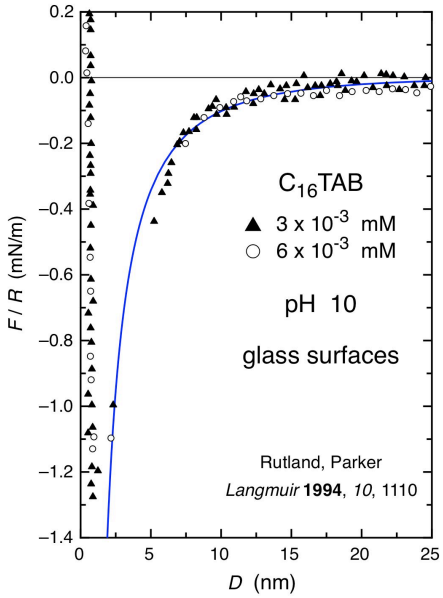

Figure 4: Normalized forces between two silica glass spheres (radius ~2 mm) in 3 x 10^{-6} (triangles) and 6 x 10^{-6} M (circles) $C_{16}TAB$ solutions at pH 10 (adjusted with addition of 2.6 x 10^{-4} M NaOH) as a

function of their separation after 14 h of equilibration (measured by means of the MASIF technique; adapted from Fig.4 of ref. 75). Within the same framework as recalled in Fig.3 the solid line shows the numerical fit to the experimental data using eqn.1 with κ^{-1} *= 20.5 nm and A = 0.23 mN/m.*

Thanks to the Derjaguin equivalence (eqn.2)[84] the results should thus be independent of the force-measuring technique used and direct comparison between measurements with different instruments should be valid for the same investigated system. Therefore their comparison would be of valuable insight likely to lead to strengthen our interpretation. All data reported by the two techniques (MASIF[74,75], colloid probe AFM[94]) use glass materials as supporting substrates, even though one is aware of their possible existence in different varieties. In the former reports the sphere-sphere geometry was used with glass spheres of $R \sim$ 2 mm whereas in the latter the interaction was measured between a flat and a sphere made of identical glass with $R \sim 0.1$ mm. Note that in most of the results discussed here surface deformation effects may be ignored except for measurements of the pull-off force or adhesion force from which it is common to infer the surface or interfacial energy γ (we postpone this discussion for a future article). All measurements show a marked decrease in the attraction range when the ionic strength becomes higher, obtained either upon salt addition or pH change, with the decay length of the attraction being simply $\kappa^{-1}/2$. In agreement with our former investigation upon salt addition[94], a similar effect is also observed when the surface charge of the underlying substrate is changed (upon pH variation), provided the charge balance between positive $C_{16}TA^+$ ions and the negative charges on the supporting glass is maintained to zero (overall charge-neutral C_{16}TAB-coated walls). Thus, the magnitude of the attraction not only increases with the ionic strength, but its related numerical prefactor A is found to be exactly proportional to the ionic strength of the bulk solution (slope 1.0 ±0.1 in a log-log plot; Fig. 5) over three decades. It increases by 2 orders of magnitude over this range. Therefore the measured force is in remarkable accordance with theoretical calculations of the interaction between two surfaces bearing adsorbed ion pairs[93,95], generalizing and strengthening our electrostatic mechanism suggested earlier[94].

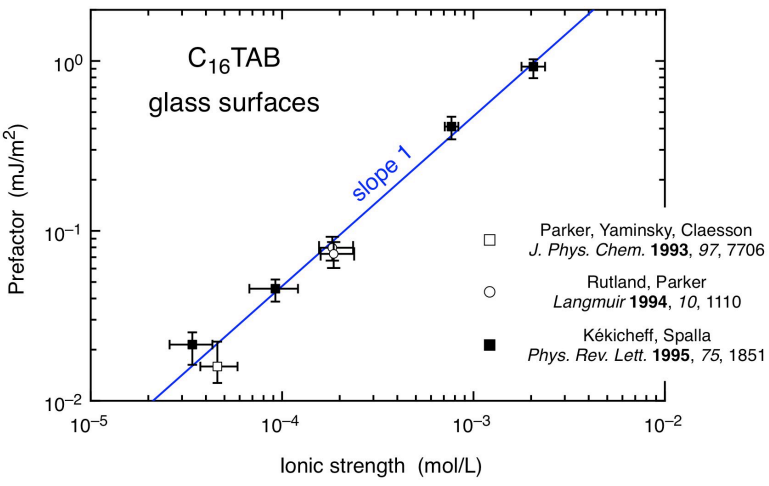

Figure 5: Variation of the prefactor A of the force law (eqn.1) with the ionic strength of the aqueous C_{16}*TAB solution (inferred from the fits of Figs. 3 and 4 and from ref. 94). The prefactor is expressed in energy per unit area through the Derjaguin equivalence (eqn.2)[84] in order to compare the data obtained between glass substrates in the sphere-sphere geometry[74,75] and those measured in the sphere-flat geometry[94]. The error bars represent the uncertainty of the fits for the different solution conditions.*

3 – 2 – Physically adsorbed double-chained-surfactants by deposition on substrates

Having demonstrated the role played by the lateral inhomogeneities along the hydrophobic film of surfactant-coated substrates in equilibrium with aqueous surfactant solutions, we have the idea that something is there, that is valuable. To generalize to other situations encountered with macroscopic substrates made hydrophobic, we pursue our investigation with still physically adsorbing surfactant systems, but this time the surfactants are highly insoluble in water and cannot exchange with the bulk composed of water molecules and small ions only (protons, hydroxide ions, (hydrogen) carbonate ions due to the presence of CO_2 dissolved in water, dissociated ions of the added salt). Such hydrophobic films are built by dip-coating or by Langmuir-Blodgett deposition.

The most common used Langmuir-Blodgett (LB) film for surface force measurements is the double-chained cationic dimethyldioactedecylammonium bromide (DODABr) or acetate (DODAA) deposited onto mica,[72,168-177] which is the preferred substrate when using the interferometric SFA. The smooth planar surface and well-defined crystal structure of muscovite also offer an ideal substrate for these dialkyldimethylammonium ions for which the cross-sectional area of the dialkyl moiety as well as the diameter of the lyophilic headgroup match the available area (0.48 nm^2) per charge on the mica surface very well. It was confirmed by XPS[178] and by Near edge x-ray absorption fine spectroscopy (NEXAFS)[179] that densely packed and highly ordered monomolecular films are formed on mica. X-ray diffraction reveals that the average molecular axis of the alkyl chain is inclined to the mica surface by ~50°.[180] Hydrophobic DODAA films were also produced on mica by adsorption from cyclohexane.[90,181] Thus, mica sheets mounted on the SFA hemicylinders were dipped into warm (≈ 50 °C) cyclohexane solutions containing 0.2 mM DODAA. After having allowed the surfactant to adsorb, the surfaces were successively washed with cyclohexane, dried, and then treated with warm water (≈ 60 °C) prior to force measurements at room temperature. Despite being deposited by different techniques, the chain order parameters of these monolayers are essentially the same.[182]

With a measured thickness ~2 nm in both methods (LB and dip-coating), the deposited monolayer is hydrophobic, having an advancing contact angle around 94°, and stable in bulk aqueous electrolyte solutions at moderate ionic strength. At high electrolyte concentrations the monolayer-covered surface becomes unstable, as recognized early by Claesson *et al.*.[168] In many studies the coated-mica surfaces were reported as weakly charged. A certain amount of variability in the apparent surface charge and the contact angle of water on the surfaces depending on deposition conditions was found. In the following we consider only the situations where the coated-mica surface is reported to be electrically neutral. However, the low value of the receding angle (50-70°) hints at heterogeneity of the deposited layer.

Figure 6 shows the force-distance profiles between two DODABr-coated mica surfaces (prepared by LB deposition) immersed in pure water.[171,173,174] As before (see § 3-1) the law given by eqn.1 describes the attraction with a reasonable agreement. Because of the scatter in the experimental data, fitting to more accurate parameters of the expected law does not visibly change the results. The latter are also compared with those obtained by dip-coating preparation of the mica surface.[90] Despite differences in the procedure for forming the hydrophobic films on the mica surfaces, in the choice of acetate rather than bromide counter-ion for the double-chained surfactant, and in the method for measuring the interaction profiles (the second one being the derivative (Fig.7) of the first one (Fig.6)), the ultimate results are comparable (Fig. 7).

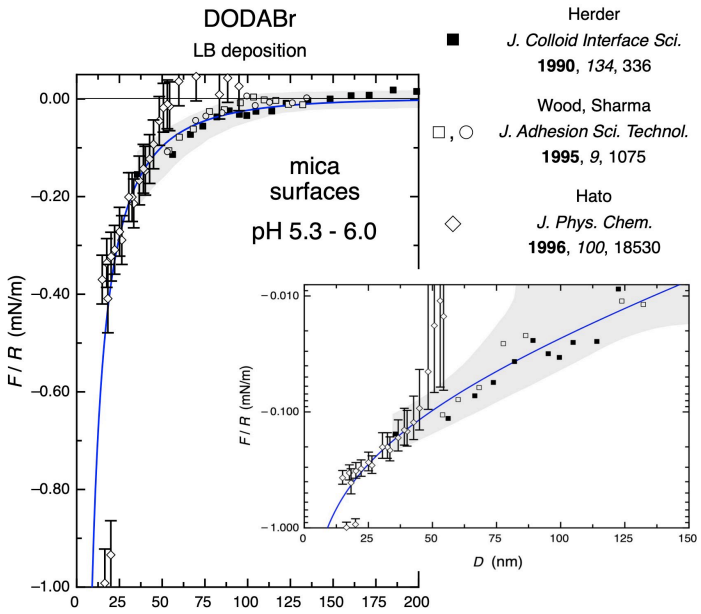

Figure 6: Surface forces between two DODABr-coated mica surfaces immersed in pure water (hydrophobic monolayers deposited by LB). The force F, normalized by the local radius of curvature of the two crossed hemi-cylinders (R ~ 2 cm), is measured as a function of the surface separation D by the SFA technique, with a zero-distance set at contact between the hydrophobic layers in water (original data from Fig. 1 of ref. 171, Fig. 1 of ref. 173, Figs. 2 and 4 of ref. 174). The estimated uncertainty in the force measurement is indicated by the shadowed area as reported in the original work[171] and by the error bars inferred from the scatter in the data points when different cantilever spring constants were used[174]. The very attractive forces measured at the shortest separations (Fig.4 of ref. 174) were not used for the analysis as the Derjaguin equivalence[84] is not fulfilled due to the deformation of the surfaces[103,104]. Within the same framework as recalled in Fig.3 the solid line shows the numerical fit to the experimental data using eqn.1 with κ^{-1} = 135.4 nm and A = 0.15 mN/m.

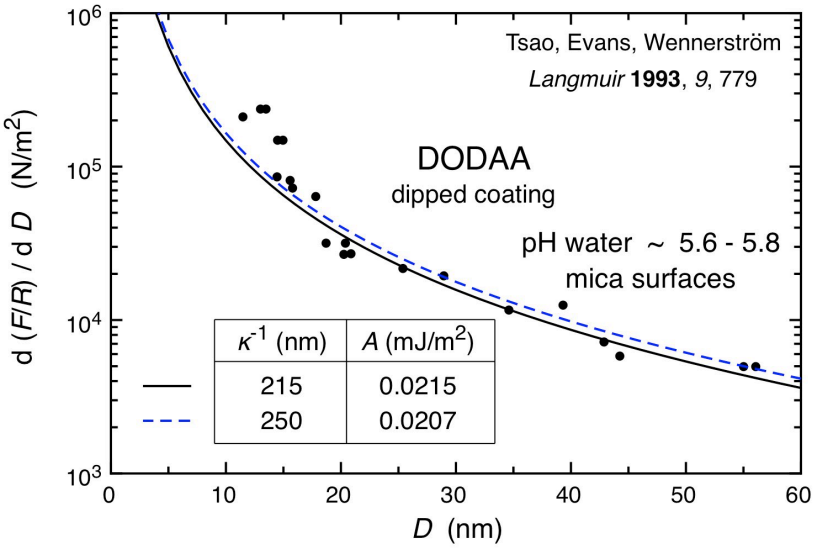

Figure 7: Interactions between two DODAA-coated mica surfaces immersed in pure water (hydrophobic layers produced by adsorption from cyclohexane after dip-coating). A variable double-leaf spring is used for the SFA measurements (gradient method; experimental data from Fig.1 of ref.

90). The monolayer contact position is set to be the zero in separation. The solid lines show the numerical fit to the experimental data using the derivative of eqn.1 with 2 sets of possible parameters.

Interestingly, the same authors investigated the effect of salt addition on the interaction, in the presence of 1:1 electrolyte (NaCl) and 2:2 electrolyte ($MgSO_4$).[90] Their experimental measurements, reproduced respectively in Figures 8 and 9, show that as the salt concentration is increased, both the range and the magnitude of the attraction are reduced. The authors fitted their data to a double exponential, with adjustable amplitudes and decay lengths. The double exponential was considered to be a convenient representation of the data, but, as in any of other articles using a similar analysis, there has never been a physical motivation and theoretical justification for such a functional form. Actually such a hazardous method always winds up with ambiguities. As an illustration, we have noted the surprising conclusion that the same four parameters were used for fitting the data obtained in "pure" water and in 10^{-5} M NaCl solution — a procedure justified by possible contamination.[90] In fact, the observed small difference between the two measured sets of data is all too real. A careful comparison reveals that the two force profiles evolve differently with the surface separation. The difference, which was claimed, in itself, marginal, is actually well described once a strong theoretical basis, as given through eqn.1, is established.

Here with eqn.1 we have fit all of the data reported in both 1:1 and 2:2 electrolytes, with only one parameter, the prefactor A, since the screening length κ^{-1} is taken from known ionic strength. The above provisions for the numerical fits are similar, if not identical (as in Figs. 4-7). Note that the range of small separations (typically $\kappa D \lesssim 1$) remains out of our focus (range over which the forces become more attractive and often deviate from the asymptotic law). The results, Table 1, and Figures 8 and 9, give easily as good fits to data as the original four-parameter picture (Figs. 1 and 3 of ref. 90). Again the decay length of the attraction is found to be governed by the ionic strength of the electrolyte solution, being simply $\kappa^{-1}/2$. The inclusion of the prefactor analysis indicated above in the text (§ 3-1, Fig. 5) would shed light on the relevance of the experiments.

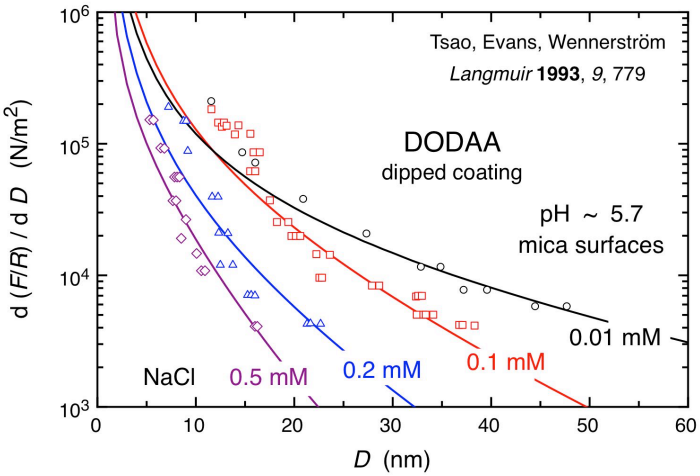

Figure 8: Interactions between two DODAA-coated mica surfaces immersed in 1:1 electrolyte (NaCl) measured by the gradient method (experimental data from Fig.1 of ref. 90). The monolayer contact position is set to be the zero in separation. The solid lines show the numerical fits to the experimental data using the derivative of eqn.1 with fitting parameters reported in Table 1.

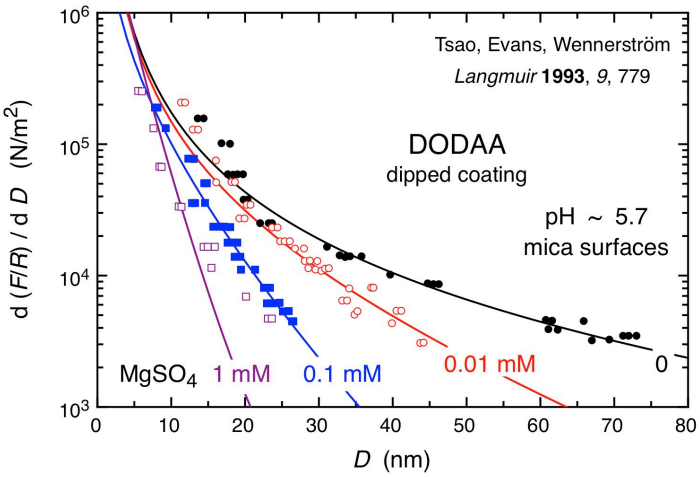

Figure 9: Same as in Fig.8 but for DODAA-coated mica surfaces immersed in 2:2 electrolyte ($MgSO_4$) (experimental data from Fig.3 of ref. 90).

Thus the effect of the ionic strength on the prefactor A of the force law (as inferred from the fits using eqn.1) is reported in Figure 10. Again the variation fulfills the expectations of the theoretical framework with scaling as the ionic strength over three decades (slope 1.0 ±0.1 in a log-log plot; Fig. 10). However, a number of important qualifications are required if the results are to be seen in the right light. In the absence of added salt, the ionic strength is uncertain as the pHs of the different experiments were not measured or not reported by the different experimental groups. Possibility that impurities corresponding to a $\sim 10^{-5}$ M concentration in conductivity water have also been invoked with honesty by some authors.[90] Therefore the group position of these data points on the left side of the x-axis may be in error. Nevertheless, even in the absence of experimental artifacts, the leveling-off of the prefactor at vanishing salt concentration is expected for films with defects at small spatial scales in their lateral structure (this will be discussed in details in § 4). The measurements performed at the highest NaCl concentrations deserve also comment, as the two corresponding data points appear laid outside the straight line. Our fits confirm the expected Debye screening length (see Table 1), but the force magnitude is below the expected theoretical one at these ionic strengths. The perceived impossibility of aligning these last two points in the 1:1 electrolyte series with all the other ones provides a possible explanatory link with film instability. Indeed, the authors have noted that the monolayers in low concentrations of salt ($\lesssim$ 0.1 mM) remained stable for at least 24 h but not at higher concentrations (~8h). With measurements carried out at least 2 h after the salt injection was made, confidence in these results cannot be built. Several arguments advocate for film metastability and degradation with time. First, it is known that chloride ions may lead to degradation of the silver layers which are evaporated onto the back of each mica sheet and form the optical cavity in the interferometric SFA.[183] In the occurrence of such events, cracks develop, solvent penetrates lifting the mica sheets around the edges: as a result a repulsive background is induced. Secondly, complementary techniques (Brewster angle microscopy (BAM), wetting studies, AFM, SFA) confirmed that deposited DODA monolayers onto mica have a rather limited stability when exposed to electrolyte solutions.[175] This thorough investigation showed that the breakdown of the film is accelerated at the three-phase contact line of a salt solution, and occurs more rapidly and more severely at higher ionic strengths. With transient vapor cavities forming between the surfaces on separation, the films become locally damaged when brought into contact successively on the same position as it is carried out with the gradient method for measuring force-distance profiles. Ultimately the film can almost be completely stripped from the mica surface.[118]

Whatever the deterioration of the surface at high salt concentration leads to (formation of multimolecular aggregates on the surface, presumably of a loose and disordered structure[175]; ion exchange of the salt ions with the surfactant cations[118]) these two force data are unreliable. And our own analysis gives rise to reasonable grounds to suspect that the deviation from the expected straight line in the log-log plot of Fig.10 would be relevant to a film instability. Therefore we will not pay too much attention to these two data points (displayed in light grey in Fig.10).

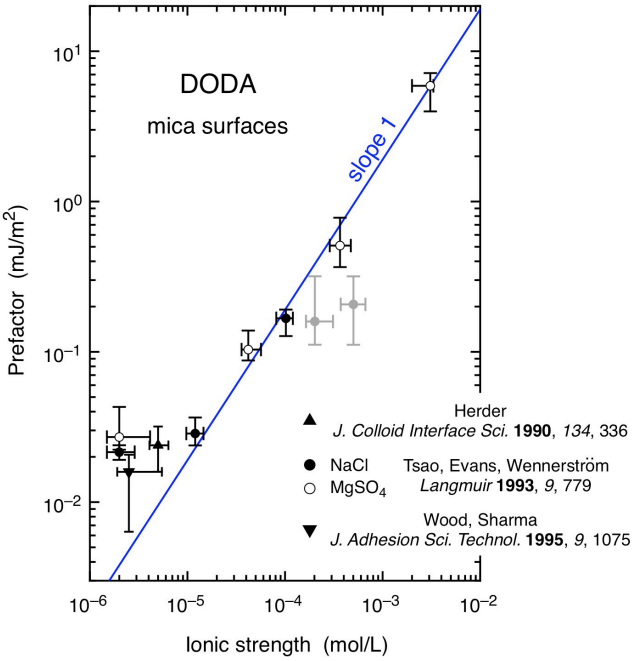

Figure 10: Variation of the prefactor A of the force law (eqn.1) with the ionic strength for the interaction between DODA-coated mica surfaces immersed in aqueous electrolyte solutions (inferred from the fits of Figs.6-9). The prefactor is expressed in energy per unit area through the Derjaguin equivalence (eqn.2)[84]. The error bars represent the uncertainty of the fits for the different solution conditions. See also detailed comments in the main text for the data points that do not sit on the straight line.

Table 1: Pseudoexponential fit (eqn.1) for interactions between two hydrophobic DODAA-coated mica surfaces upon addition of NaCl and $MgSO_4$ at 25°C (Figs.7-9; experimental data from ref. 90).

salt		Concentration (mM)	Debye length[a] (nm)	κ^{-1} (nm)	A^b (mJ/m²)
water	Fig. 7	0	190 – 250 [c]	215 – 250	0.0215 – 0.0207
	Fig. 9	0	190 – 250 [c]	250	0.0223
NaCl	Fig. 8	0.01	88.2	88.0	0.0318
		0.1	30.4	30.6	0.1512
		0.2	21.6	21.0	0.0748
		0.5	13.7	11.0	0.2387
$MgSO_4$	Fig. 9	0.01	47.8 [d]	47.8	0.1035
		0.1	15.9 [d]	15.9	0.5093
		1	5.5 [d]	5.7	5.8887

[a] calculated at the ionic strength, I, of the solution at temperature T, by taking into account the activity coefficients of the ions of valence z. The extended Debye-Hückel for activity was used: $\log f = -Az^2\sqrt{I}/\left(1 + Ba\sqrt{I}\right)$ with $A = 1.82 \times 10^6 (\varepsilon T)^{-3/2}$ (where ε is the dielectric constant), $B =$

$503(\varepsilon T)^{-1/2}$ and a (nm) related to the hydrated ion size.[184-186]

[b] expressed in energy per unit area by converting the normalized force through the Derjaguin approximation[84] (eqn.2).

[c] pH assumed to be around 5.7, but the value was not reported explicitly by the authors.

[d] symmetrical divalent electrolytes are not completely dissociated even at moderate (~10 mM) concentrations, but the possible complication of ion pairing giving rise to species of differing charges does not occur.[187]

3 – 3 – Self-assembled monolayers: hydrophobic silylated films chemically adsorbed on substrates

New ways of constructing monolayers made of long aliphatic chains chemically anchored to a substrate have emerged in the last decades giving a powerful alternative to the Langmuir-Blodgett technique. These self-assembled monolayers (SAM), as first reported by Bigelow *et al.* in the late 1940s,[188] are supposed to be stronger and more resistant than their LB counterparts physically linked to the surface only. A large variety of surfaces can be modified by silane molecules, as for instance silica and glass,[12,13,30-38,189-199] silicon,[191,200-211] metal,[191,195,212] or mica[76,77,208,213-227]. Depending on its chemical nature (terminal functionality; length and saturation/unsaturation of the alkyl chain), the silane transforms those substrates into hydrophobic or hydrophilic substrates. But other factors are also known to have an influence on the ultimate wettability of the film-coated substrate: these include the mixture with different molecules, the reaction conditions (gas phase versus liquid phase; type of solvent), the water content on the surface (hydration), the concentration of the organosilane, reaction temperature, time of treatment, and the surface modification procedure for covalently bind the molecules to the underlying substrate.

Variability in film quality is the main drawback in using organosilane-treated surfaces for force measurements. This variability is often attributed to the self-polymerization of the organosilane giving rise to an ill-defined, polymerized silane coating.[195] These irregularities are often observed for surfaces with high contact angles and are mostly favored when the interface of the hydrophobic substrate is inhomogeneous. This is for instance the case of silica surfaces silanated with octadecyltrichlorosilane (OTS)[33] for which domains (clusters of lateral size ~ 20 nm x 40 nm with height ~2–4 nm) that are formed during the adsorption process[33,228] favor the presence of (nano)bubbles sitting at the inhomogeneities of the hydrophobic monolayer inducing cavitation and bridging effect between opposite approaching hydrophobic surfaces. Thus, in most of the force-distance profiles reported for silanated substrates, the curves are stepped.[32] As stated in the Introduction, this bridging force produced by the intervention of bubbles attached onto hydrophobic surfaces cannot be regarded as the true meaning of the hydrophobic attraction.[14] Here in this section, our focus is rather on surfaces with a hydrophobizing agent bonded chemically onto the surface on which there were neither nanobubbles nor a gas phase. Concerning the force measurements between chemisorbed surfaces in the absence of preexisting or induced bubbles, we note that many experimental difficulties have been encountered, as summarized below.

Mica is attractive as it can be cleaved to form molecularly smooth surfaces over several square centimeters and thus is ideal for use as a substrate for force measurements. However, deposition of alkylsilanes, mostly OTS and *n*-octadecyltriethoxysilane (OTE), on mica, resulted in unstable films in aqueous solutions. For instance, the OTE monolayer self-assembled on bare mica was shown to be only weakly physisorbed and not chemically anchored to the substrate at all.[229] As a result, and contrary to early claims of robustness, the film swells at high humidity[229] and may detach ultimately in aqueous solutions from the mica sheets used in the SFA experiments. The stability of alkylsilane monolayers on mica can be

increased by activating mica with an argon/water vapor plasma[76,77] to introduce hydroxyl functional groups on the surface that could potentially form covalent bonds with the silane monolayer. Nevertheless, despite surface anchoring sites induced by plasma activation, the produced layer, securely bound to the mica substrate, appears to be not robust enough in aqueous salt solutions. The contact angle decrease with prolonged exposure to water indicates water penetration into the monolayer and a structural evolution of the film with the presence of aggregates. Therefore, these surfaces are not fully suitable for SFA studies:[15] the use of mica for preparing hydrophobic SAM surfaces has been abandoned since, and all other studies of the hydrophobic attraction between silanated surfaces have employed silica as the substrate.

On the surface of silica, glass, and quartz, the presence of silanols allows the deposited silane SAM films to be strongly anchored. Surface homogeneity, smoothness, and film stability are achieved provided that the silanation process has been carried out with optimized conditions[191,192,194] and long equilibration since the reactions at the solution – solid interface may be slow in the later stages (sometimes more than 1 day is required to achieve maximum bonding density[209]). However, attempts at measuring attractive forces between such hydrophobic layers are frequently frustrated by the surface charge developed at their interfaces in aqueous solutions. To our best knowledge, only two sets of direct force measurements have been reported between SAM monolayers for which charge neutrality of the hydrophobized substrate has been ensured by the authors in aqueous electrolyte solutions. Figure 11 presents the force-distance profile measured between crossed filaments in quartz that were hydrophobized with a difunctional silane in vapor.[30] As noted by other groups the vapor phase method is one of the cleanest method to obtain high yield surface modification with short alkyl chain reagent.[192,194] The hydrophobic surface exhibits large contact angles with water (advancing contact angle ~100°) in agreement with other reports using the same preparation method for similar silanes.[209] The hysteresis with water is high (contact angle hysteresis ~20°): it has been interpreted as resulting from the disordered structure of the methyl groups (molecular roughness and rigidity).[209] As recalled in § 2, the negative feedback loop allows a direct measurement of the attractive force without any data treatment. The experimental data which represent the interaction operating at equilibrium between the two surfaces are well fitted by eqn.1 at the ionic strength of the solution (solid line).

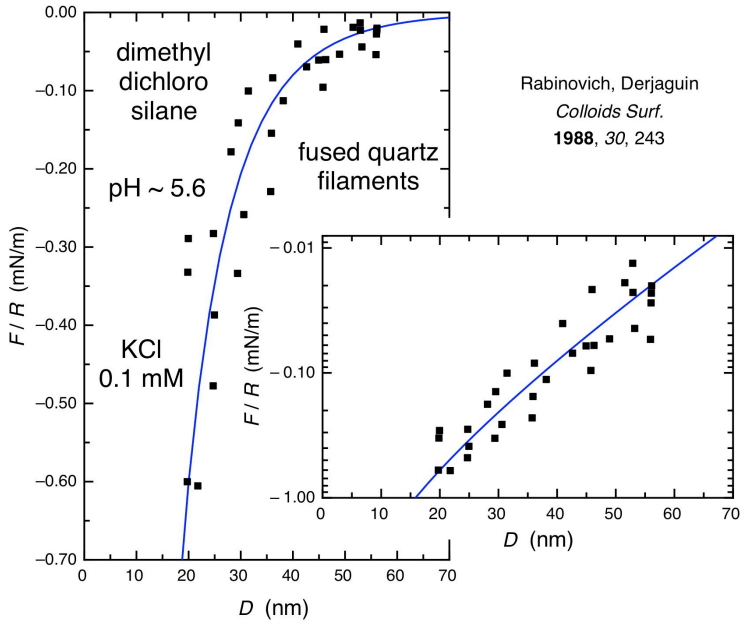

Figure 11: Surface forces between two hydrophobized quartz filaments immersed in 0.1 mM KCl aqueous solution (fused quartz hydrophobized by chemically adsorption of a difunctional silane $Si(CH_3)_2Cl_2$ in vapor for 24 h). The attractive force F, normalized by the local radius of curvature of the two crossed filaments (R ~ 1 mm), is measured as a function of the surface separation D by an optoelectronic negative feedback loop technique, with a zero-distance set at contact between the hydrophobic layers in solution (uncertainty ~ 1 nm; data extracted from Fig. 1 of ref. 30). The solid line shows the numerical fit to the experimental data using eqn.1 with κ^{-1} = 30.1 nm and A = 3 mN/m.

The results obtained in the sphere-sphere geometry for glass surfaces hydrophobized by a monofunctional fluorocarbon silane[31] are presented in Figure 12. Despite being highly hydrophobic, the surfaces are also charged in pure water. This indicates that parts of the underlying glass substrate must be accessible to the aqueous environment (see § 4). And yet the advancing (~98°) and receding contact angles (~80°) with water have values similar to the difunctional silane reported in Fig. 11. This is another illustration where contact angles cannot give any indication about the structure and morphometry of the adsorbed hydrophobic film.[73] Other techniques must be called for (for instance ellipsometry and X-ray reflectivity were used to investigate the structure of the same film[203]). Note that the advancing contact angle is relatively insensitive to the extent of coverage once it has exceeded a certain fraction of the surface. Thus, incomplete coverage could still result in a near maximum advancing angle even though the receding angle is low. By adjusting the pH to the isoelectric point (pH ~ 2) a pure attraction was measured by means of the MASIF technique. Figure 12 reports the measurements carried out after 24 h. We have discarded the measurements reported by the authors[31] immediately after pH adjustment for two reasons. First, it is likely that those data were not collected at the thermodynamic equilibrium. Indeed, the decay-length inferred from a fit (not shown) using eqn.1 would correspond to a solution that would be at pH ~ 3 and not 2. A nonequilibrium situation is actually often encountered when opposite SAM coated-surfaces are separated by a thin aqueous gap: a proper solution mixing requires time to ensure thermodynamic equilibrium once solution conditions are changed in situ. Secondly, the argument advocated by the authors for explaining the reductions in both the attraction range and the adhesion force, namely the possibility of silane hydrolysis, is ruled out by others (see for instance refs. 12,230): these changes are not due to the loss or removal of methyl groups from the surface but rather to the presence of physically bound water molecules and hydrated ions. Again, insufficient equilibration does not allow thermodynamic equilibrium to be achieved. Conversely at the thermodynamic equilibrium, the experimental data are well fitted by eqn.1 (solid line, Fig. 12). The comparison between the two silanated systems (Figs. 11 and 12) shows that the two prefactors scale with the ionic strength as expected (eqn.3). Their values are discussed in § 4 and reported in Fig. 13.

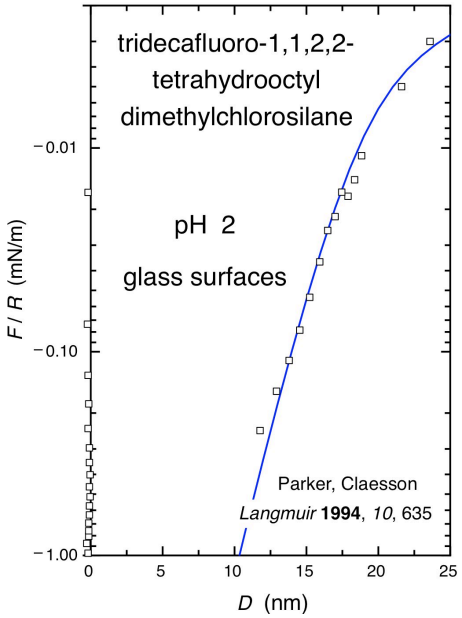

Figure 12: Surface forces between two silanated glass surfaces immersed in aqueous solution (glass spheres hydrophobized with a fluoro monofunctional silane $CF_3–(CF_2)_5–(CH_2)_2–Si(CH_3)_2Cl$ in vapor). The attractive force F, normalized by the local radius of curvature of the two spheres (R ~ 2 mm), is measured as a function of the surface separation D by the MASIF technique (data extracted from Figs. 1 and 2 of ref. 31). The reported distance in the force profiles is relative to the position of the hard wall reached in each force curve (uncertainty ~1 nm). On each glass surface the thickness of the silane layer is 1–2 nm. The solid line shows the numerical fit to the experimental data using eqn.1 with κ^{-1} = 3.7 nm and A = 180 mN/m.

4 – Discussion

The experimental data reviewed in this article were obtained from many different systems and with use of four different force measurement techniques. We have reported force-distance profiles solely to measurements carried out between two *identical* surfaces. Likeness for interacting surfaces is settled twofold: not only the underlying solid substrates are strictly identical in terms of homogeneity, smoothness, and physicochemical properties (such as wetting), but also their hydrophobic coating is prepared and achieved by means of the same procedure. This avoids complications that may arise from heterosurface interaction. Within this framework, the three main classes of substrates rendered hydrophobic are illustrated by specific examples: The hydrophobic film is composed of physically adsorbed surfactants, either by deposition of highly insoluble surfactants in aqueous solutions (double chain surfactants deposited by dip-coating and Langmuir-Blodgett), or in equilibrium with bulk surfactant solutions (water soluble single alkyl chain surfactants having adsorbed from bulk), or is built by chemical adsorption of self-assembled monolayers (silane). Attention was paid to select experiments performed with *quenched* systems (at least over the time frames of the experiments), in the absence of nanobubbles (either preexistent or induced by the mechanical contact of the two opposite substrates), and when *thermodynamic equilibrium*, *film stability*, and *charge neutrality* in aqueous solutions are ensured. Finally, all the attractive profiles reported in Figs.3,4,6-9,11,12 are the raw measurements collected by the authors while avoiding any data treatment. We emphasize that the attraction observed is obtained *directly* from the measurements. This point is important: the results are for purely attractive force curves, not being obscured by any other repulsive forces, and these authors have not needed to subtract any electrical double layer or hydrodynamic (repulsive) contributions. Moreover, the interacting surfaces interact in a *well-defined geometry*. With the three main possible geometries set by a sphere interacting with another sphere or with a flat, or between two crossed-cylinders, the local radii of curvature of the extended surfaces investigated lie in a large range spanning four decades from a few centimeters down to a few micrometers. In conclusion, our data selection have overcome all the ambiguities that often lead to differing outcomes of experiments with the suggestion that "the systems and methods are fraught with complexity and incidental issues that must be carefully considered in the analysis of such data".[17] By transforming the force normalized by the local radius of curvature of the surfaces into the free energy of interaction per unit area between two parallel flat surfaces (eqn.2),[84] we can now proceed to a comparison between the measurements collected with the different instruments on this large variety of systems.

All the measured attractive force-distance profiles present a remarkable similarity. At large surface separations they decay exponentially with a decay length simply equal to half the Debye screening length at the ionic strength of the solution (Figs. 3,4,6-9,11,12 and Table 1). Provided the surfaces keep their overall electric charge neutrality, this generic outcome of

a $\kappa^{-1}/2$ decay length arises whether the solutions are composed of small ions, free ionic surfactant molecules, their mixture, and upon ionic strength change achieved with salt addition, pH variation, or higher surfactant concentrations. The decay length $\kappa^{-1}/2$ is a rigorous result for the asymptotic behavior of the interaction free energy between planar surfaces infinite in extent (eqn.3). Note that the $e^{-2\kappa D}/(2\kappa D)$ functional form is also the asymptotic law found for dispersion forces[231] that decay twice as fast as the usual electrical double layer between charged surfaces where the screening of the electrolyte remains governed by the Debye length κ^{-1}. Indeed, electrostatic fluctuations at one surface induce a response at the other that returns and interacts with the original fluctuations: as a result, the distance traveled is actually twice the separation *D*. The magnitude of the energy due to dispersion forces scales with the total ionic density, ρ_{tot}. However, at the equilibrium it is bound by an upper universal value given by eqn.3 with α = 2 for planar homogeneous surfaces attracting only through dispersion forces.[231] Strikingly, all the measured attractive forces between overall charge-neutral hydrophobic macroscopic surfaces exceed the van der Waals force by some two orders of magnitude. For instance, for the physically adsorbed C_{16}TAB single chain cationic surfactant on opposite negatively charged mica or silica substrates, the prefactor is found ~75 larger (α = 153 ± 16; Fig. 5). As proposed earlier[94] and now convincingly generalized with our analysis of all the measurements performed by others and reported in § 3 within the aforementioned framework with its six rigorous experimental criteria, one is forced to reconsider an electrostatic mechanism in searching for an acceptable description of the long-range attraction operating between similar, overall charge-neutral, hydrophobic extended surfaces.

In contrast to the measured rate of decay that is in accord with theoretical macroscopic considerations (through a dielectric continuum for describing the electrolyte solution confined between identical, infinite planar walls), it appears that the long-range attraction between these two electrical neutral (on average) walls will be perceived and apprehended in its essence only if the prefactor *A* given by eqn.1 is understood through a microscopic description.

At this stage we recall that several theoretical approaches have been attempted even if the experimental accord with eqn.1 and eqn.3 had not been recognized yet.[94] One early suggestion was a phenomenological mean-field analysis involving an enhancement of the hydrogen bond network of the fluid close to hydrophobic surfaces.[86] This structural mechanism that would propagate layer-to-layer with a correlation length of some 15 nm in the direction normal to the surfaces appears unrealistic in view of the rapid decay of surface order-induced effects (not more than a few molecular diameters[232-235]). A different line of thinking started out from the observation that a vapor cavity forms around the contact region when two hydrophophic surfaces have come into mechanically contact.[169] This spontaneous cavitation suggests that the aqueous film between the surfaces is metastable.[91,92] Conceptually, the capillary evaporation or cavitation which will occur if the spinodal of the confined fluid is approached[91] is equivalent to a capillary condensation from an undersaturated bulk gas.[236] Most certainly the water density can be reduced at a hydrophobic substrate / water interphase as suggested theoretically.[237,238] However, molecular dynamics simulations indicate a water depletion region extending at most 0.3 nm from the hydrophobic surface[239] while neutron[240-243] and x-ray[244,245] reflectivity have suggested a 1– to 4–nm depleted region where the water density at the interface is reduced. In addition, grazing incidence small angle neutron scattering (GISANS)[243] and x-ray reflectivity at high resolution[244,245] have shown no major role to the presence of dissolved gas in the aqueous solution while it might have reasonably been imagined that hydrophobic surfaces would have enhanced nucleation of gas in their vicinity and hence would have affected the solvent density. This is in line with our own conclusions inferred from refined refractive

measurements of the thin aqueous layer confined between two hydrophobic mica surfaces rendered hydrophobic by C_{16}TAB surfactant adsorption from bulk solution.[101] All these experimental results rule out the suggested metastability of the film due to its confinement as a mechanism (spinodal approach[91]; lateral enhancement of density fluctuations in the aqueous film[92]) to explain the long-range attraction observed between hydrophobic extended surfaces. Note also that explanations based on the instability of the amount adsorbed when the surface separation is varied[78,79,246] do not hold when the hydrophobic films are quenched, and even if the latter were not, the calculations would require a too large shift in the origin of the separation[79].

In searching for a microscopic origin of the magnitude of this long-range attraction, electrostatic correlation forces have been considered independently.[87-89] Attard proposed that the hydrophobic surfaces induce anomalous polarization fluctuations in the adjacent water layers.[87] His model predicts an attractive interaction with a decay length of $\kappa^{-1}/2$, due to coupling between these fluctuations. However, as pointed out by Podgornik[89] the anomalous dielectric behavior of the solvent close to the surface assumed by Attard[87] cannot give rise to an attraction stronger than the dispersion forces calculated within the Lifshitz theory.[85,165-167,231]

An alternative explanation suggests that the metastability of the confined aqueous film induces nonequilibrium states with local fluctuations of adsorbed charges that would correlate electrostatically on the opposing hydrophobic surfaces, and an attraction with a decay length of $\kappa^{-1}/2$ results.[88,89] Note that this model strongly differs from other suggestions related to surface heterogeneities forming patches or periodic lattice structures for which the asymptotic law $e^{-2\kappa D}/(2\kappa D)$ is not recovered by the theoretical calculation assuming in-plane lateral dipolar interactions[90] or very large surface charge densities in the heterogeneities.[247] Indeed, within a framework where the affinity of the ions adsorbing to the surface is the cause of the enhancement of the attraction, it is not sufficient to keep the surfaces overall electrically neutral, but also to recognize that eqn.3 remains strictly valid for small densities of charge only.[93-95] Thus, when the surface density Σ_i of an adsorbed pair of ions of type i ($\Sigma_i^+ = \Sigma_i^- = \Sigma_i$ for cations and anions of the same pair i at concentration ρ_i) is larger than $\rho_i\kappa^{-1}$, the magnitude of the interaction energy which reads[94]

$$E = -64\pi k_B T L_B^2 \left(\Sigma_i + \Sigma_j + \cdots - \frac{\rho_{\text{tot}}}{2\kappa}\right)^2 \frac{\exp(-2\kappa D)}{2\kappa D} \qquad (4)$$

should still be bound by the universal limit of the van der Waals attraction. This is why no enhanced attraction beyond classical dispersion forces (and eventually capillary bridging due to the presence of nanobubbles) is observed between hydrophobic substrates with homogeneous surfaces or when the adsorbed density is high (for instance polymer surfaces[19,24-29]). For all the fits reported in § 3, the condition $\Sigma_i < \rho_i\kappa^{-1}$ is fulfilled. For illustration, with glass substrates having adsorbed C_{16}TAB surfactant from bulk at the highest ionic strength (2.3 mM KBr added; see Fig.5 and ref. 94), eqn.4 reproduces the magnitude of the measured attraction with a value of 8.6 x 10^{-3} pairs of adsorbed ions per nm^2, still a factor 2 smaller than $\rho_{\text{tot}}\kappa^{-1}$= 1.8 x 10^{-2} nm^{-2}.

Models with random inhomogeneously charged layers have also recently attracted much attention (for a recent review see ref. 70). The disorder in the surface charge can be annealed or quenched experimentally. The annealed case was illustrated by purposely building charge-mosaic structures using the adsorption of the cationic C_{16}TAB surfactant on negatively charged mica surfaces.[248] The procedure consisted of several steps. First, mica surfaces were immersed in the surfactant solution above the cmc for about 2h before fast

withdrawing (1.0 ± 0.5 mm/s rate). Then, the surfaces were rinsed by dipping in pure water for 20 s to remove unbounded molecules, and ultimately replaced inside the apparatus filled with pure water for force measurements.[249] Tapping AFM mode imaging reveal series of irregular patches surrounded by areas of regular height, which is likely to be bare mica as stated by the authors. The patches have lateral dimensions in the range 50-400 nm and different thicknesses: some are roughly the double that of the monolayer while other ones are much higher with heights 10 times more, around 20 nm (see the topographic AFM images reported both in ref. 249 (Fig.7) and in ref. 248 (Fig.1)). Force measurements show that the surfaces jump into contact from separations in the range 30-50 nm, suggesting the occurrence of an attraction stronger than van der Waals. The observation that two hydrophilic surfaces covered by domains of positive and negative charge may attract each other across electrolyte solutions is in agreement with earlier suggestions.[2,247] As pointed by the authors[248] the "mosaic-charge surfaces are clearly hydrophilic rather than hydrophobic and so differ conceptually from the earlier work[15]". The same group investigated also the quenched case by using a similar quaternary ammonium surfactant but with a longer chain (C_{18}TAB).[250] A random mosaic of positively charged bilayers on a background of negatively charged bare mica was created following the same procedure. Nevertheless the distribution of surface charge was effectively quenched by means of a rapid shear motion between the surfaces. The measured strong and long-range attraction, analyzed within the Poisson-Boltzmann framework, was suggested by the authors to arise from an asymmetry in the interaction between like and oppositely charged domains across electrolyte solutions. The authors also stated that their "results have clear implications for understanding long-ranged attractions between the large class of surfaces made hydrophobic by surfactant monolayers that subsequently rearrange into positive and negative charged domains".[250] In their model, domains large compared to the intersurface separation are invoked, since small patches (equivalent to quenched disorder of small uncorrelated domains) have no effect on the net interaction at the mean-field level.[251] Despite a qualitative agreement, Monte Carlo simulations[252] and theoretical calculations[70] contrast quantitatively the model of Silbert *et al.* In addition, they found an attraction decaying at large separations as $e^{-\kappa D}$ where κ^{-1} is the Debye screening length and the asymptotic law $e^{-2\kappa D}/(2\kappa D)$ could not be recovered.

Israelachvili and collaborators[253] suggested a general interaction potential for describing the interactions between both hydrophobic and hydrophilic surfaces. There, the interaction energy, E, is exponentially decaying with separation, D, as $E = -2\gamma_i H_y e^{-D/D_H}$ where γ_i is the interfacial tension of the interacting surfaces and H_y a nondimensional parameter. This interaction law naturally accounts for repulsive interactions ($H_y < 0$) between hydrophilic surfaces, generally known as hydration forces, which exhibit decay lengths, D_H, in the range of 0.1-1.0 nm [253-261] (longer decay-lengths, up to 2.0 nm, have also been reported, but they are believed to have been effected by other incidental experimental issues such as additional repulsive forces arising from the deformation[103,104] of the surfaces in the SFA experiments). Similar values for the decay lengths are invoked for describing the interaction between hydrophobic surfaces ($H_y > 0$ for partially hydrophobic surfaces with the maximum $H_y = 1$ for fully hydrophobic surfaces). According to these authors, "the exact value of D_H is dependent on the chemical and morphological identity of the surfaces and the solution conditions." [253] This model would be interesting for describing the interaction at small intersurface separations. These authors further hypothetized that the longer ranged nature of the force is due to "long-range correlations from dipolar, angular, or proton-hopping correlations among water molecules confined between hydrophobic surfaces".[253] However, the asymptotic law $e^{-2\kappa D}/(2\kappa D)$ could not be recovered.

For all the models with specific surface ion adsorption[88,89,93-95] that fulfill the twofold conditions emphasized above (electrical charge neutral surfaces on average; small densities of

adsorbed charges) the presence of heterogeneities on the surface is essential and represents an inescapable reality, otherwise the prefactor in eqns.3,4 will be bound by the universal van der Waals attraction. And this is absolutely the case: for the three classes of hydrophobic systems investigated in § 3, surface heterogeneities are evidenced at the thermodynamic equilibrium. Thus:

(i) the adsorbed C_{16}TAB molecules build patchy patterns composed of connected monolayer-like stripes as evidenced by AFM imaging using the recent PeakForce Tapping (PFT-AFM) mode that allows fragile structures to be imaged with the lowest possible applied force.[82] In the narrow concentration regime of charge inversion the mica surface coverage is ≈2/3 and the adsorbed film composed of alternating bare and covered patches without any long-range order behaves as a *quenched* system. Lateral correlations along the hydrophobic surfaces are also revealed by x-ray scattering using our recent SFAX on synchrotron radiation facilities (Fig.2 and ref. 98). The measured correlation length ($\xi \approx 12$ nm) in the equatorial plane is substantiated by theoretical calculations predicting a microstructured film such a layer with an array of holes or stripes alternating covered patches and bare substrate as a result of the energetic balance between electrostatics and line tension (ref. 98 with further details in a forthcoming article). Actually similar patchy patterns are expected at any charged substrate-water interfaces adsorbing oppositely charged surfactants,[262] although it is likely that larger lateral structures would form on a substrate with a smaller original surface charge (such as silica, glass, or quartz, compared to mica). Contrary to the fairly complete picture that recently emerged for the film structure and the organization of the C_{16}TAB surfactant aggregates adsorbed on mica[82] a precise determination of the morphometry is still lacking for C_{16}TAB films coating silica, glass, or quartz. Nevertheless reflectometry measurements point towards similar conclusions: patchy mono- and bilayered-like C_{16}TAB aggregates have been inferred from neutron reflectometry on silica[129,131-133] and on quartz[130] along the same lines as recent x-ray reflectometry on C_{16}TAB-coated mica[134,135,263]. Note also that structural inhomogeneities have also been reported by AFM imaging of silica plates having adsorbed C_{16}TAB (at ≈1/15 cmc [122]) or similar alkyltrimethylammonium surfactants (for instance C_{18}TACl at concentrations where long-range attractive forces are observed[264,265]).

(ii) the films of water insoluble double chain surfactant DODABr deposited on mica are heterogeneous on three length-scales.[175] During deposition a stick-jump behavior of the meniscus induces a large-scale heterogeneity of approximately 1 mm measurable in wetting studies. Brewster angle microscopy (BAM) reveals that the film is composed of domains on a length-scale of 20-50 μm while AFM imaging shows the presence of small isolated holes.[175] The small defects have an average diameter of ≈30 nm with a center-center distance of ≈100 nm (without any long-range ordering) and make up a small portion of the total area (≈10%). Despite the possible presence of some overtuned cationic $DDOA^+$ adsorbed molecules, the conditions are not ripe for a surface charge reversal. Indeed, the charge on the bare mica exposed by the holes is not compensated by small cations such as H^+ (since H^+ is a potential determining ion for mica[53,266]), bound K^+ (from the surface dissociation of mica immersed in aqueous solution), or Na^+ ions brought by the added salt. Negative zeta potentials have indeed been measured independently, but the low value (-8 to -10 mV) indicates a surface ionization extremely small (in the range 0.02–0.5%) and thus a negligible contribution, if any, of an electrical double layer repulsion to the measured force, as reported in Figs.7-9.[90]

(iii) the chemically anchored SAMs on solid substrates present heterogeneities at different spatial scales. Buckling of thin 2D films into the third dimension may arise. For instance for OTS-coated silicon wafers, buckling results in domains of 4–9 μm size welded together with a wave amplitude of the height profile ranging between 0.25 and 2 nm as evidenced from grazing incidence x-ray scattering and AFM imaging.[204] It is now well established that the morphology of the final grafted monolayer depends on a variety of

parameters (dryness and pretreatment of the substrate, gas phase versus liquid phase, adsorbate concentration and type of solvent, soaking time, temperature, etc.) with a self-assembling occuring in two main steps, a physical two-dimensional ordering with its associated lateral diffusion of adsorbed molecules (analogous to Langmuir monolayers)[202,206,207] followed by a chemical grafting. Islands formation (dotlike or multiply branched islands) is commonly observed, as demonstrated by a combination of different techniques (such as AFM,[33,196,198,201,206-208,210,211,215,217,221,224,226,228] ellipsometry,[196,203,208,211] X-ray photoelectron spectroscopy (XPS),[196,209-211] FTIR,[191,194,208,224,228] x-ray reflectivity[200,203,204]). Thus the process of SAM formation consists of interfacial adsorption of silane molecules uniformly distributed over the substrate in a disordered manner, followed by nucleation and growth of densely-packed 2D molecular aggregates (islands), which later fill out and rearrange into a final highly ordered film structure through coalescence and Ostwald ripening process (the growth of large islands at the expense of small islands). Therefore heterogeneities and defects are inevitably present in the ultimate film, even if high surface coverage can be achieved. The layer is invariably inhomogeneous and consists of numerous small islands (size ranging from ~100–200 nm [196] to 1–2 μm [206]) on high density silane, interspersed with a low-density disordered phase. Even when the coverage is almost complete, prior gaps (~50 nm) between domains remain along the film, as indicated by faint scars in the AFM images.[215] The coexistence of different structural domains, which is clearly evident in the experimental IR spectra and grazing incident x-ray diffraction, does not exclude subtle structural transitions within each domain, resulting in certain distributions for the domain height, the chain tilt angle, the packing density, or in-plane intermolecular ordering.[205,208] Furthermore, defects within the films could occur from missing molecules, incorrectly oriented molecules, or otherwise physically adsorbed molecules.[211] Thus, the presence of pinholes in the monolayer has been revealed by AFM (their diameters range from several nanometers to about 100 nm [201,211,217,221]) and interpreted as resulting from imperfections of the lateral siloxane bonds in the network, that is between physically adsorbed silane molecules which are not covalently bound to neighbor chemically adsorbed molecules to the surface. In summary, self-polymerization (or oligomerization) of dichlorosilanes (such as the one used in Fig.11) and trichlorosilanes leads to the formation of ill-defined and nonuniform films because cross-linking impacts steric constraints in forming uniformly packed and covalently bonded silane monolayers on the surface. This explanation is substantiated by theoretical work showing that if every OH surface group reacted with the silane, a densely packed monolayer could form provided there was no cross-linking.[267] With cross-linking by forming Si–O–Si bonds between the silane species, steric repulsions between the hydrocarbon chains of the silanes would preclude the formation of a densely packed monolayer. Reactive silanes bearing a single chloro group (such as the one used in Fig.12) can bind with either the surface or another silane molecule, but not to both. This lack of extensive cross-polymerization between silane molecules would lead to a near-perfect film on the substrate (free of defects). Unfortunately the monofunctional silane-coated glass surface is again less than ideal: the film contains also defects and heterogeneities. In that case the failure might be attributed to blocking of surface reactive silanol sites through adhesion of dimerized or miss-oriented silane molecules.[192,194,211] Thus dimethylalkylmonochlorosilanes are not able to cover a silica surface at a surface density equal to the surface hydroxyl density.[267]

In summary the aforementioned short review points out that hydrophobization of substrates by adsorption of surfactants or SAMs cannot provide an ideal hydrophobic interface free of structural irregularities and defects when in contact with aqueous solutions. Nor is it a question of whether this results from the displacement of some adsorbed molecules (those which precisely make the surface hydrophobic) upon change in the intersurface separation. The key point is that some inhomogeneities and multiscale defects are always

present in the ultimate structure of the hydrophobic coated-substrate, even for systems prepared at the thermodynamic equilibrium and in a quenched state. With this evidence encountered for the three classes of substrates rendered hydrophobic we now have an essential observation in the appraisal of the long-range attraction operating between hydrophobic, overall charge-neutral, extended surfaces. The consequences of this non-ideal film structure are twofold:

First it explains the leveling-off at vanishing ionic strength, where the measured decay length becomes independent of salt concentration (Fig. 10). As pointed earlier[88,89] there is a surface contribution to the total free energy of the system in addition to the contribution of the fluctuations of the local electrostatic potential around its mean field profile to the energy of interaction of the two opposed surfaces. Two competing characteristic lengths are at play, the bulk Debye screening length, κ^{-1}, and the finite size, L, of the domains over which charge fluctuations can occur. Actually, due to the microstructure of the hydrophobic film composed of hydrophobic patches, exposed portions of the underlying substrate not covered by the coated film, and multi-scale defects, there is a distribution of lateral lengths. Here, the smeared-out spatial distribution is reduced in an effective characteristic length, noted L (further details will be given in a forthcoming article). The rate of decay of the attraction between two overall charge-neutral microstructured like-surfaces is determined by the smaller of these two lengths since the asymptotic intersurface separation regime scales as $\exp\left(-2\sqrt{\kappa^2 + (\pi/L)^2}D\right)$.[87-89] At high ionic strength, the screening by the electrolyte makes the effective size of the domains irrelevant and the decay length is half the Debye screening length, $\kappa^{-1}/2$. Conversely, at low ionic strength, the limitation is the size of the effective domains, and the interaction becomes independent of salt concentration. This leveling-off is evidenced for deposited films composed of water-insoluble double-chain surfactants where force measurements at vanishing ionic strengths could be carried out (Fig. 10): below 10^{-5} M, i.e. for Debye screening length larger than ~90 nm, the defects and the structural inhomogeneities of the coated film become relevant for the effective measured decay length as their characteristic size is smaller or of the order of κ^{-1}. For the case of physically adsorbed single chain surfactants in equilibrium with surfactant bulk solutions, the ionic strength is too high (> 2.2 x 10^{-5} M) for such a regime to take place (Fig. 5).

Secondly it appears that the surface response of the system immersed in electrolyte solutions is crucial. As already emphasized, the overall charge-neutral surfaces are not highly conductive planes that would allow for long-range lateral correlations.[268] Furthermore there is neither large surface dielectric response nor large surface charge densities, otherwise those situations would merely lead to the screened dispersion forces between ideally polarizable half-spaces, that are still a couple of orders of magnitude away from the actual measured attraction.[88,89,93-95] Clearly no enhanced attraction can arise between substrates with homogeneous structural surfaces with perfect lateral mobility of adsorbed ions or surfaces with sufficient surface charge densities that counterions in their vicinity may lead to a kind of conducting surface. Here, the distinctive feature is to recognize the role of the structural defects along the surfaces that allows surface domains to fluctuate independently. Within this framework each opposing surface can adsorb small ions of both sign: the (small) surface charge density can fluctuate around zero with desorption into or adsorption from the aqueous electrolyte solution (provided the condition $\Sigma_i < \rho_i \kappa^{-1}$ is fulfilled). Local surface ion concentrations can correlate along the surfaces over small lateral spatial extent *only*, and without propagation of any long-range order. This limited lateral correlation induces a larger strength and longer range than the usual dispersion forces. Building on the evidence that in the three classes of substrates rendered hydrophobic all the coated films possess inhomogeneities and multiscale defects we can forge a new momentum, a genuinely

comprehensive approach for the appraisal of the magnitude of the long-range attraction operating between two such essentially electrically neutral like-surfaces. For all the systems reported in § 3 the prefactor A of the force law (eqn.1) is proportional to the ionic strength over three decades (slope 1.0 ± 0.1 in a log-log scale as illustrated in Figs. 5 and 10) in agreement with the theoretical expectations.[93-95] The physical meaning of the position (magnitude) of the corresponding straightline may be discussed as follows.

Although of comparable magnitudes the long-range attractive energies exhibit differences, suggesting a common underlying mechanism (adsorption/desorption of pairs of positive and negative ions exchanging with the bulk;[94] redistribution of the ions when the structures on opposing surfaces start to interact;[98] surface charge fluctuations and ionic correlations) but where the microstructure of the hydrophobic surface is the one which ultimately tunes both the range and magnitude of the attraction. Thus, the interfacial energies would reflect, not only the strength of ion adsorption to the surface, but also the morphometry of the hydrophobic layer. The quenched microstructuration is essential since the small ions adsorb into and desorb from the local surface inhomogeneities and defects present. Note also that the quenched case is very sensitive to counterion release contrary to the annealed case that mainly involves polarization effects somewhat similar to van der Waals interactions.[68] From the perspective of ion correlation fluctuations resulting from the presence of structural inhomogeneities and defects along the hydrophobic films, one can now compare the respective strength of the force law operating in the three systems reported in § 3.

A traditional criterion for assessing the hydrophobicity and quality of films is through water contact angle measurements (advancing (θ_a) and receding (θ_r) contact angles, and their hysteresis). Although this approach is a major topic of discussion, we have decided to go along and to overcome the caution precisely pointed out for the three aforementioned systems,[73,174,209] since only a qualitative hierarchy was sought for tabulating the hydrophobized substrates with ranks. The silane-based films produce the highest contact angles with θ_a = 100° and θ_r = 80° for dimethyldichlorosilane on quartz (Fig. 11)[30] and even higher for the fluorosilane on glass (θ_a / θ_r = 98° / 80° (Fig. 12)[31] and 110° / 90° in another report by the same authors[32]). The monolayers of the double-chain DDOABr surfactant, deposited on mica surfaces by the Langmuir-Blodgett method, exhibit advancing and receding contact angles respectively in the range 95-97° / 56-57° (Fig. 6).[171,173] Contact angle data were not reported in the original publications for the DDOAA film deposited on mica from organic solutions (Figs. 7-9).[90,181] The self-assembled monolayers of single-chain-water-soluble surfactants in equilibrium with surfactant solutions, such as C_{16}TAB (Figs. 3-5), produce the lowest contact angles (θ_a / θ_r = 94° / 45° for C_{16}TAB on mica[73] and 90° / 40° on glass[94]). All the contact angle values with water indicate that the covered substrates are, as expected, hydrophobic, with advancing contact angles falling in the range 90 -115° expected for hydrocarbon-terminated surfaces. The three systems can consequently be rank ordered based on these observations. This hierarchical classification appears also to be in accordance with the surface coverage of the underlying substrate by the hydrophobic film: The silylated glass substrates to which the highest rank is attributed are also well coated (surface coverage ~90%). They are followed by the DODABr monolayer LB films (~80% [175]) and then by the C_{16}TAB surfactant monolayered-like films (~65% [82]) labeled with the lowest rank.

Owing to the foregoing, the surface density of defects may emerge as a useful parameter for relating changes in surface chemistry to the strength of the hydrophobic interaction energy. The latter is signaled by the respective positions (magnitudes) of the straightlines that relate the proportionality of the prefactors A with the ionic strength (Figs. 5,10). In fact, it would appear that the surface coverage governs the trend when comparing the different systems, but qualitatively only. Indeed, in the result set ranked in accordance with the labeled rank of the three systems, the positions (magnitudes) of the corresponding three

straightlines are in the ratio 1 : 0.40 : 0.11. Consequently, a quantitative analysis requires special precautions, as different surface densities and distributions are intertwined. On the one hand, ions of both signs adsorb and desorb on each surface. Therefore the fluctuations in local surface ion concentrations can correlate over small regions along the same surface. This will amount in the prefactor through the surface densities Σ_i for the pairs of ions of type i as given by eqn.4.[94] However, these expressions for the interaction free energy are general results for uncharged symmetric bodies that are equally applicable to hydrophobic and to hydrophilic surfaces. What distinguishes the different situations are the morphometries of the coated films with their inherent microstructuration specific of a peculiar system. Thus the prefactor dependence on the surface densities Σ_i only, as given by eqn.4, is too simplistic and must be refined. In the water slab, the dielectric constant becomes anisotropic.[69,71] For a given system, its local profiles parallel and perpendicular to the surface together with the charge-charge correlation function will depend on the distributions not only in size but also in shape of the covered / noncovered domains and imperfections (defects, holes, clusters, etc.) along the surface. An illustrative example is given by the monolayered-like structure built up by the adsorbed C_{16}TAB surfactant where elongated shapes of connected stripes are formed at the thermodynamic equilibrium (see Fig. 2 of ref. 82). Note also that when domains of different sizes coexist, the largest ones will give the longest range in the electrostatic interaction. We postpone the presentation of the film microstructuration for a forthcoming article. At the present stage the prefactor data measured for the three systems (Figs. 5, 9-12) have been simply renormalized by the square of the surface density of the defects. We have assumed that for each system, the surface coverage varies little with the ionic strength. This hypothesis is reasonable since the systems are in a quenched state (at least over the time frames of the experiments) and the surfaces remain essentially charge-neutral over the whole range of ionic strength reported in § 3. Remarkably all the data fall onto a single master curve (solid line, Fig. 13), at least in nonvanishing electrolyte. As discussed above for the situation at very low salt content, the prefactor becomes independent of the bulk Debye screening length because the effective size associated to the defects and the structural inhomogeneities of the coated film becomes dominant in the interaction.

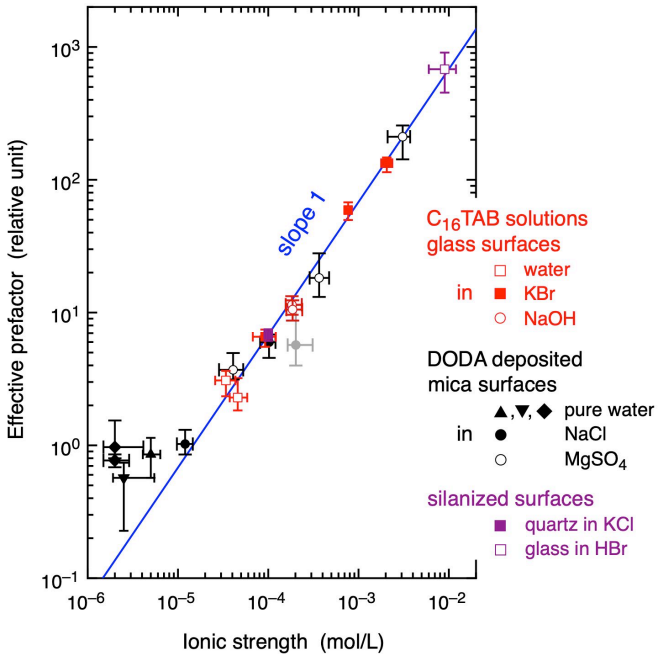

Figure 13: Effective prefactor A of the force law (eqn.1) with the ionic strength for the interaction between identical substrates rendered hydrophobic by three different procedures: chemically adsorbed silane layers on glass and quartz (data points in purple; from Figs. 11,12) and physically adsorbed surfactant either by deposition on mica (by Langmuir-Blodgett or from organic solution for the water-insoluble double-chain DODA; data points in black from Fig. 10) or by adsorption on glass from aqueous surfactant solutions (single-chain $C_{16}TAB$ in equilibrium with surfactant solutions at different pHs and univalent salt content; data points in red: from Fig. 5). By renormalizing the prefactor with the square of the surface density of the defects in the hydrophobic film coating the supporting substrate, all the data points lie on a single master curve (solid line of slope 1.0 ± 0.1 on a log-log scale). At vanishing salt concentration the interaction becomes independent of the bulk ionic strength being dominated by the structural inhomogeneities along the layers: the prefactor levels off (see main text).

The fact that the renormalized prefactors appear to collapse onto a single curve suggests a striking degree of similarity between hydrophobic surfaces interacting at large separations. It appears that the microstructuration is the spatial source for providing regions where ions adsorb from and desorb into the aqueous solution. At the same time the film morphometry sets more than an upper limit for the ionic surface density but also restricts the lateral correlations among the adsorbing charges along the same surface. These two boundary cases, beyond which the interaction free energy would saturate with an attraction that would revert to the form characteristic for the screened van der Waals interaction between polarizables bodies, highlight the essential requirement of a microstructuration at the hydrophobic surfaces: when the latter is quenched and at the thermodynamic equilibrium, it makes the walls to appear inhomogeneous, and a long-range strongly attractive force can be generated, otherwise none of this would beam in. The establishment of a single master curve, on which all the measurements lie, is of valuable interest as it allows comparison between systems and prediction of the interaction strength for other ones not investigated yet. Indeed, our experimental framework substantiated by theory shows that all the force-distance profiles depend on one parameter only. The rate of decay is predicted from macroscopic considerations (the known ionic strength of the solution) whereas the magnitude of the attraction results from microscopic mechanisms governed by the microstructuration of the hydrophobic layer. The film morphometry characterizes a given hydrophobic system and hence one is only reduced, for instance, to determining its form factor (particularly the form factor of the charge-charge correlation function) to foresee the strength of the attraction as the prefactor amounts up to a multiplicative constant only.

5 – Conclusion

The wealth of experimental data reported for the last decades has been beneficial for allowing the researchers to possibly identify the mechanism inducing a very long range strongly attractive force between extended hydrophobic surfaces in aqueous solution. So far it has been believed that there is no single mechanism that can account for the diversity of behavior observed with differently prepared hydrophobic surfaces. This statement is correct when it includes the observed attractions of variable strength and range, due to the presence of (nano) bubbles. Nevertheless the observed force is not more than a capillary force resulting from the gaseous bridge formed from the coalescence of nanobubbles at the liquid-hydrophobic interface. Thus, the so-called “hydrophobic” force measured in such cases appears to be a misleading term.[14,43] Therefore there remains a plethora of experiments using different model hydrophobic surfaces at the solid-water interface that indeed showed a variety of results, sometimes contradictory or controversial. All the reviews point out the

discrepancies highlighting possible interferences to the measurements and to the experimental procedure for preparing the hydrophophic surfaces.[14-17] Nevertheless, when these interferences to the measurements are eliminated, the experimental situation becomes extremely illuminating. Thus, on the contrary, the present work shows that actually all the systems behave and interact in a similar manner at least at large separations.

None of these conclusions would have been possible if the experimental framework for the appraisal of the interaction potential operating between extended hydrophobic surfaces was not fulfilled sixfold. We have narrowed our focus to systems with *no submicroscopic bubbles* (preexistent or induced). We considered solely *symmetric* hydrophobic surfaces that were prepared with the same procedure on identical underlying substrates and in a *well-defined interacting geometry* (crossed-cylinders; sphere-flat; sphere-sphere). They are all surface-stable entities in aqueous electrolyte solutions and are at the thermodynamic equilibrium in a *quenched* state. The hydrophobic surfaces are *overall charge-neutral*, and the force-distance profile is obtained *directly* (no or negligible hydrodynamic contribution). Therefore there is no additional interaction to be considered except the ever-present dispersion forces. The results presented in this article concern experiments carried out by other groups and by us with the goal to encompass the three main categories of substrates rendered hydrophobic: substrates coated with a hydrophobizing agent bonded chemically onto the surface and surfaces obtained with surfactant monolayers physically adsorbed from solution to deposited ones.

Our present work has not dwelled on the overall dependence, but rather has focused on the long-range attraction and the asymptotic regime at large separations. Remarkably the range and the decay of the attraction emerge directly from the known screening length of the electrolyte aqueous solution. Our early result for single-chain surfactants physically adsorbed on substrates in equilibrium with surfactant aqueous solution at different salt contents[94] is now generalized for the two other classes of systems, namely physically adsorbed monolayers of water-insoluble double-chain surfactants deposited by LB or from organic solutions and chemically anchored silane films. It is concluded that the measured decay lengths are in accord with theoretical predictions, simply being half the Debye screening length, $\kappa^{-1}/2$, at least in non vanishing electrolyte. More precisely, the interaction energy scales as $A\exp(-2\kappa D)/2\kappa D$ at large separations. Taken together with the prefactor A scaling as the ionic strength, the interaction energy between overall charge-neutral extended hydrophobic surfaces is demonstrated to have an electrostatic origin in all the systems. Building on our challenging experiment that has recently allowed force measurements to be coupled with x-ray solution scattering under controlled nano-confinement,[98] the microstructuration of the adsorbed film has emerged as an essential feature in the molecular mechanism for explaining the enhancement of the prefactor A compared to the usual screened van der Waals attraction. The adsorption of pairs of positive and negative ions on small islands along the interface, the fluctuation of the surface charge density around a zero mean-value with desorption into or adsorption from the electrolyte solution, the local surface ion concentrations that correlate along the surfaces over small lateral spatial extent only, the redistribution of counterions when the aqueous gap between the two opposing surfaces is varied, all contribute and are tuned finely by the inhomogeneities and defects present in the coated film along the hydrophobic surface. As a result the strength of the hydrophobic interaction potential can be compared between different systems. Indeed, the prefactors are related not only to the affinity of the adsorbed ion pairs for the walls and to their surface density, but also to the surface density of defects in the microstructure. As we showed, a universal single master curve encompassing all the systems can be established for the magnitude of the interacting energy. In summary, in contrast to the rate of decay that is predicted from macroscopic considerations (the ionic

strength of the solution), the magnitude of the attraction results from microscopic mechanisms governed by the microstructuration of the hydrophobic layer.

This article offers finally a simple explanation for the long-range attraction between macroscopic hydrophobic interfaces immersed in aqueous solutions. We have emphasized the important role driven by the microstructuration of the adsorbed layer. The electrostatic response explains the difference between hydrophobic and hydrophilic surfaces. It is likely that the nature of the fluid within several molecular layers of the interface plays also an important role.[61-71] In addition changes in the dynamics of the aqueous solution due to its confinement and low affinity of the water to the surfaces have been suggested as inducing an additional contribution to the disjoining pressure.[96,97] Whatever the interaction energy at short separation is, our present description demonstrates that inhomogeneities and defects at these interfaces account qualitatively and quantitatively for the properties and interactions, at least at large separations, of such substrates. Electrically neutral surfaces, if they are ideally homogeneous, will not induce any enhancement of the prefactor and the force will revert to the usual screened van der Waals attraction. This statement must of course be moderated in the case of divalent (or multivalent) ions where ion-ion correlations may induce strongly short-range attractive forces between homogeneous surfaces (see for instance ref. 183 for a direct experimental measurement of this additional attraction at small intersurface separations, and references therein). Similarly to examples of colloidal behavior where traces of surface-active substances can control the surface behavior and hence the macroscopic properties of the colloidal dispersion,[2,269] here the behavior lies on the deviation from ideality for the surface structure. Small number of surface defects (even of the order of 10%) and structural inhomogeneities may induce very large effects as illustrated precisely by the long-range strongly attractive force that exceeds the ubiquitous van der Waals attraction by some two orders of magnitude. By coupling force measurement and structural determination under controlled nano-confinement[98] we have sought here to establish the relationship force – distance – structure. Our method should prove beneficial to many studies, which heretofore have often relied on assumptions and indirect measurements. Thanks to our recent developed SFAX, coupling the Surface Force Apparatus technique with x-ray scattering at small and wide angles, the previous confused puzzle of wildly varying observations has been rationalized. It sets the bases of a solid ground to pursue along this new avenue opened from now on.

Acknowledgments

The author would like to thank Albert Johner for enlightening discussions on the subject. The technical staff and scientists of the Institut Charles Sadron (Strasbourg, France), the French national SOLEIL (Saint-Aubin, France) and European (E.S.R.F., Grenoble, France) synchrotron radiation facilities and neutron facility (I.L.L., Grenoble, France) are gratefully thanked for their participation and help in the design, build-up and development of advanced setups for the experiments.

References

1 - Israelachvili, J. N. *Intermolecular and Surface Forces. With Applications to Colloidal and Biological Systems.* Academic Press: New York, 1985.

2 - Evans, D. F. & Wennerström, H. *The Colloidal Domain: Where Physics, Chemistry, Biology, and Technology Meet* (Advances in Interfacial Engineering), Wiley-Blackwell, 2nd ed., 672 pp. (1999).

3 – Ninham, B. W. & Lo Nostro, P. *Molecular Forces and Self Assembly: In Colloid, Nano Sciences and Biology*. Cambridge Molecular Science Series, 365 pp., Cambridge University Press: Cambridge, England, 2010.

4 - Tanford, C. *The Hydrophobic Effect: Formation of Micelles and Biological Membranes.* Wiley: New York, 1973

5 - Tanford, C. Hydrophobic Effect and Organization of Living Matter. *Science* **1978**, *200* (4345), 1012-1018.

6 - Ninham, B. W.; Larsson, K.; Lo Nostro, P. Two sides of the coin. Part 1. Lipid and surfactant self-assembly revisited. *Colloids Surf. B: Biointerfaces* **2017**, *152*, 326-338.

7 - Ninham, B. W.; Larsson, K.; Lo Nostro, P. Two sides of the coin. Part 2. Colloid and surface science meets real biointerfaces. *Colloids Surf. B: Biointerfaces* **2017**, *159*, 394-404.

8 - Kauzmann, W. Some Factors in the Interpretation of Protein Denaturation. *Adv. Protein Chem.* **1959**, *14*, 1-63.

9 - Lipowsky, R. Morphological wetting transitions at chemically structured surfaces. *Curr. Opin. Colloid Interface Sci.* **2001**, *6*, 40-48.

10 - Schulze, H. J. *Physico-Chemical Elementary Processes in Flotation.* Elsevier: Amsterdam, 1984.

11 - Fuerstenau, D. W.; Jameson, G.; Yoon, R.-H. *Froth flotation: A century of innovation*, Society for Mining, Mettallurgy, and Exploration, Inc. (SME), Littleton, Colorado (U.S.A.), 2007.

12 - Laskowski, J. Kitchener; J. A. The hydrophilic - hydrophobic transition on silica. *J. Colloid Interface Sci.* **1969**, *29*, 670-679.

13 - Blake, T. D.; Kitchener, J. A. Stability of Aqueous Films on Hydrophobic Methylated Silica. *J. Chem. Soc. Faraday Trans. I* **1972**, *68*, 1435-1442.

14 - Spalla, O. Long-range attraction between surfaces: Existence and amplitude? *Curr. Opin. Colloid Interface Sci.* **2000**, *5*, 5-12.

15 - Christenson, H. K.; Claesson, P. M. Direct measurements of the force between hydrophobic surfaces in water. *Adv. Colloid Interface Sci.* **2001**, *91*, 391-436.

16 - Meyer, E. E.; Rosenberg, K. J.; Israelachvili, J. N. Recent progress in understanding hydrophobic interactions. *Proc. Natl. Acad. Sci. U.S.A.* **2006**, *103* (43), 15739-15746.

17 - Tabor, R. F.; Grieser, F.; Dagastine, R. R.; Chan, D. Y. C. The hydrophobic force: measurements and methods. *Phys. Chem. Chem. Phys.* **2014**, *16*, 18065-18075.

18 - Hunter, R. J. *Foundations of colloid science.* Clarendon Press: Oxford, 1987.

19 - Kratohvil, S.; Matijevic, E. Stability of colloidal teflon dispersions in the presence of surfactants, electrolytes, and macromolecules. *J. Colloid Interface Sci.* **1976**, *57* (1), 104-114.

20 - Tabor, R. F.; Wu, C.; Grieser, F.; Dagastine, R. R.; Chan, D. Y. C. Measurement of the hydrophobic force in a soft matter system. *J. Phys. Chem. Lett.* **2013**, *4*, 3872-3877.

21 - Firouzi, M.; Howes, T.; Nguyen, A. V. A quantitative review of the transition salt concentration for inhibiting bubble coalescence. *Adv. Colloid Interface Sci.* **2015**, *222*, 305-318.

22 - Del Castillo, L. A.; Ohnishi, S.; Carnie, S. L.; Horn, R. G. Variation of local surface properties of an air bubble in water caused by its interaction with another surface. *Langmuir* **2016**, *32*, 7671-7682.

23 - Parker, J. L.; Claesson, P. M.; Wang, J.-H.; Yasuda, H. K. Surface forces between plasma polymer films. *Langmuir* **1994**, *10*, 2766-2773.

24 - Schmitt, F.-J.; Ederth, T.; Weidenhammer, P.; Claesson, P. M.; Jacobasch, H.-J. Direct force measurements on bulk polystyrene using the bimorph surface forces apparatus. *J. Adhesion Sci. Technol.* **1999**, *13*, 79-96.

25 - Vinogradova, O. I.; Yakubov, G. E.; Butt, H.-J. Forces between polystyrene surfaces in water-electrolyte solutions: Long-range attraction of two types? *J. Chem. Phys.* **2001**, *114*, 8124-8131.

26 - Considine, R. F.; Hayes, R. A.; Horn, R. G. Forces Measured between Latex Spheres in Aqueous Electrolyte: Non-DLVO Behavior and Sensitivity to Dissolved Gas. *Langmuir* **1999**, *15*, 1657-1659.

27 - Faghihnejad, A.; Zeng, H. Hydrophobic interactions between polymer surfaces: using polystyrene as a model system. *Soft Matter* **2012**, *8*, 2746-2759.

28 - Considine, R. F.; Drummond, C. J. Long-Range Force of Attraction between Solvophobic Surfaces in Water and Organic Liquids Containing Dissolved Air. *Langmuir* **2000**, *16*, 631-635.

29 - Stevens, H.; Considine, R. F.; Drummond, C. J.; Hayes, R. A.; Attard, P. Effects of degassing on the long-range attractive force between hydrophobic surfaces in water. *Langmuir* **2005**, *21*, 6399-6405.

30 - Rabinovich, Y. I.; Derjaguin, B. V. Interaction of hydrophobized filaments in aqueous electrolyte solutions. *Colloids Surf.* **1988**, *30*, 243- 251.

31 - Parker, J. L.; Claesson, P. M. Forces between hydrophobic silanated glass surfaces. *Langmuir* **1994**, *10*, 635-639.

32 - Parker, J. L.; Claesson, P. M.; Attard, P. Bubbles, cavities, and the long-ranged attraction between hydrophobic surfaces. *J. Phys. Chem.* **1994**, *98*, 8468-8480.

33 - Rabinovich, Ya. I.; Yoon, R.-H. Use of atomic force microscope for the measurements of hydrophobic forces. *Colloids Surf. A* **1994**, *93*, 263-273.

34 - Carambassis, A. C.; Jonker, L. C.; Attard, P. Rutland, M. W. Forces measured between hydrophobic surfaces due to a submicroscopic bridging bubble. *Phys. Rev. Lett.* **1998**, *80*, 5357-5360.

35 - Ishida, N.; Sakamoto, M.; Miyahara, M.; Higashitani, K. Attraction between hydrophobic surfaces with and without gas phase. *Langmuir* **2000,** *16,* 5681-5687.

36 - Yakubov, G. E.; Butt, H.-J.; Vinogradova, O. I. Interaction forces between hydrophobic surfaces. Attractive jump as an indication of formation of "stable" submicrocavities. *J. Phys. Chem. B* **2000**, *104*, 3407-3410.

37 - Ishida, N.; Kusaka, Y.; Ushijima, H. Hydrophobic attraction between silanated silica surfaces in the absence of bridging bubbles. *Langmuir* **2012,** *28,* 13952-13959.

38 - Soga, Y.; Imanaka, H.; Imamura, K., Ishida, N. Effect of surface hydrophobicity on short-range hydrophobic attraction between silanated silica surfaces. *Adv. Powder Technol.* **2015**, *26*, 1729-1733.

39 - Ishida, N.; Inoue, T.; Miyahara, M.; Higashitani, K. Nano bubbles on a hydrophobic surface in water observed by Tapping-mode Atomic Force Microscopy. *Langmuir* **2000**, *16*, 6377-6380.

40 - Lou, S. T.; Ouyang, Z. Q.; Zhang, Y.; Li, X. J.; Hu, J.; Li, M. Q., Yang, F. J. Nanobubbles on solid surface imaged by atomic force microscopy. *J. Vac. Sci. Technol. B* **2000**, *18*, 2573-2575.

41 - Zhang, X. H.; Zhang, X.; Sun, J.; Zhang, Z.; Li, G.; Fang, H.; Xiao, X.; Zeng, X., Hu C. H.; Fan Hu, J. Detection of novel gaseous states at the highly oriented pyrolytic graphite-water interface. *Langmuir* **2007**, *23* (9), 1778-1783.

42 - Seddon, J. R. T.; Lohse, D. Nanobubbles and Micropancakes: Gaseous Domains on Immersed Substrates. *J. Phys: Condens. Matter* **2011**, *23*, 133001.

43 - Hampton, M. A.; Nguyen, A. V. Nanobubbles and the nanobubble bridging capillary force. *Adv. Colloid Interface Sci.* **2010**, *154*, 30-55.

44 - Peng, H.; Birkett, G. R.; Nguyen, A. V. Progress on the surface nanobubble story: What is in the bubble? Why does it exist? *Adv. Colloid Interface Sci.* **2015**, *222*, 573-580.

45 – Yaminsky, V.; Ohnishi, S.; Ninham, B. W. (2001). Long-range hydrophobic forces due

to capillary bridging, in *Handbook of Surfaces and Interfaces of Materials*, edited by H. S. Nalwa, vol. 4: Solid Thin Films and Layers, chap. 3, 131-227, **2001**.

46 - Rosen, M. J. *Surfactants and Interfacial Phenomena*, 3rd ed.; John Wiley & Sons, Inc.; Hoboken, N.J., 2004, ch.3, 128 pp.

47 - Tadros, T. F. *An introduction to surfactants*, edited by W. de Gruyter GmbH, Berlin, Boston, 2014.

48 - Bakx, A.; Timmerman, A.; Frens, G. The flow of concentrated surfactant solutions through narrow capillaries. *Colloid Polym. Sci.* **2000**, *278* (5), 418-424.

49 - Eastoe, J.; Hollamby, M. J.; Hudson, L. Recent advances in nanoparticle synthesis with reversed micelles. *Adv. Colloid Interface Sci.* **2006**, *128-130*, 5-15.

50 - Bakshi, M. S. How surfactants control crystal growth of nanomaterials. *Cryst. Growth. Des.* **2016**, *16* (2), 1104-1133.

51 - Biresaw, G. (Ed.); Mittal, K. L. (Ed.), *Surfactants in Tribology*, vol. 5., Boca Raton: CRC Press, 2018.

52 - Scales, P. J.; Grieser, F.; Healy, T. W. Electrokinetics of the muscovite mica-aqueous solution interface. *Langmuir* **1990**, *6*, 582-589.

53 - Shubin, V. E.; Kékicheff, P. Electrical double layer structure revisited via a surface force apparatus: Mica interfaces in lithium nitrate solutions. *J. Colloid Interface Sci.* **1993**, *155*, 108-123.

54 - Adamczyk, Z., Bratek-Sticki, A., Zeliszewska, P., Wasilewska, M., Mechanisms of fibrinogen adsorption at solid substrates. *Curr. Top. Medic. Chem. Chem.* **2014**, *14*, 702-729.

55 - Israelachvili, J.; Pashley, R. The hydrophobic interaction is long range, decaying exponentially with distance. *Nature* **1982**, *300*, 341-342.

56 - Derjaguin, B. V.; Landau, L. Theory of the stability of strongly charged lyophobic sols and the adhesion of strongly charged particles in solutions of electrolytes. *Acta Phys. Chim. USSR* **1941**, *14*, 633-662.

57 - Verwey, J. W.; Overbeek, J. T. *Theory of the Stability of Lyophobic Colloids*; Elsevier: Amsterdam, 1948.

58 - Kjellander, R.; Marcelja, S. Inhomogeneous Coulomb fluids with image interactions between planar surfaces. III. Distribution functions. *J. Chem. Phys.* **1988**, *88*, 7138-7146.

59 - Kjellander, R.; Marcelja, S. Surface interactions in simple electrolytes. *J. Phys. (France)* **1988**, *49*, 1009-1015.

60 - Kékicheff, P.; Ninham, B. W. The double-layer interaction in asymmetric electrolytes. *Europhys Lett.* **1990**, *12*, 471-477.

61 - Kjellander, R.; Akesson, T.; Jönsson, B.; Marcelja, S. Double layer interactions in mono- and divalent electrolytes: A comparison of the anisotropic hypernetted chain theory and Monte Carlo simulations. *J. Chem. Phys.* **1992**, *97*, 1424-1431.

62 - Kjellander, R. Modified Debye-Hückel approximation with effective charges: An application of dressed ion theory for electrolyte solutions. *J. Chem. Phys.* **1995**, *99*, 10392-10407.

63 - Holm, C.; Kékicheff, P.; Podgornik, R. *Electrostatic Effects in Soft Matter and Biophysics*, edited by C. NATO Science, Series II-Mathematics Physics and Chemistry Vol. 46 (NATO, 2001), ISBN: 1-4020-0197-5.

64 - Andelman, D. *Introduction to electrostatics in soft and biological matter*, in Soft Condensed Matter Physics in Molecular and Cell Biology, edited by W. C. K. Poon and D. Andelman, Scottish Graduate Series (NATO Adv. Sci. Inst., Scottish Summer School of Physics, 2006), pp. 97–122.

65 - Bonthuis, D. J.; Netz, R. R. Beyond the continuum: How molecular solvent structure affects electrostatics and hydrodynamics at solid-electrolyte interfaces. *J. Phys. Chem. B* **2013**, *117*, 11397-11413.

66 - Kanduc, M.; Schlaich, A.; Schneck, E; Netz, R. R. Hydration repulsion between membranes and polar surfaces: Simulation approaches versus continuum theories. *Adv. Colloid Interface Sci.* **2014**, *208*, 142-152.

67 - Ghodrat, M.; Naji, A.; Komaie-Moghaddam, H.; Podgornik, R. Strong coupling electrostatics for randomly charged surfaces: antifragility and effective interactions. *Soft Matter* **2015,** *11*, 3441-3459.

68 - Adar, R. M.; Andelman, D.; Diamant, H. Electrostatic attraction between overall neutral surfaces. *Phys. Rev. E* **2016**, *94*, 022803.

69 - Schlaich, A.; Knapp, E. W.; Netz, R. R. Water dielectric effects in planar confinement. *Phys. Rev. Lett.* **2016**, *117*, 048001.

70 - Adar, R. M.; Andelman, D.; Diamant, H. Electrostatics of patchy surfaces. *Adv. Colloid Interface Sci.* **2017**, *247*, 198-207.

71 - Schlaich, A.; dos Santos, A. P.; Netz, R. R. Simulations of nanoseparated charged surfaces reveal charge-induced water reorientation and nonadditivity of hydration and mean-field electrostatic repulsion. *Langmuir* **2019**, *35*, 551-560.

72 - Christenson, H. K.; Claesson, P. M.; Parker, J. L. Hydrophobic attraction: A reexamination of electrolyte effects. *J. Phys. Chem.* **1992**, *96*, 6725-6728.

73 - Kékicheff, P.; Christenson, H. K.; Ninham, B. W. Adsorption of cetyltrimethylammonium bromide to mica surfaces below the critical micellar concentration. *Colloids Surf.* **1989**, *40*, 31-41.

74 - Parker, J. L.; Yaminsky, V. V.; Claesson, P. M. Surface forces between glass surfaces in cetyltrimethylammonium bromide solutions. *J. Phys. Chem.* **1993**, *97*, 7706-7710.

75 - Rutland, M. W.; Parker, J. L. Surface forces between silica surfaces in cationic surfactant solutions: Adsorption and bilayer formation at normal and high pH. *Langmuir* **1994**, *10*, 1110-1121.

76 - Parker, J. L.; Cho, D. L.; Claesson, P. M. Plasma modification of mica: Forces between fluorocarbon surfaces in water and a nonpolar liquid. *J. Phys. Chem.* **1989**, *93*, 6121-6125.

77 - Parker, J. L.; Claesson, P. M.; Cho, D. L.; Ahlberg, A.; Tidblad, J.; Blomberg, E. Plasma modification of mica. *J. Colloid Interface Sci.* **1990**, *134*, 449-458.

78 - Pethica, B. A. Adsorption equilibria in surface force balance studies. *Colloids Surf A* **1995**, 257-264.

79 - Podgornik, R.; Parsegian, V. A. Forces between CTAB-covered glass surfaces interpreted as an interaction-driven surface instability. *J. Phys. Chem.* **1995**, *99*, 9491-9496.

80 - Waltermo, A; Sjöberg, M.; Anhede, B.; Claesson, P. M. Adsorption of an ethoxylated amine surfactant on mica and its effect on the surface forces. *J. Colloid Interface Sci.* **1993**, *156*, 365-376.

81 - Subramanian, V.; Ducker, W. Proximal adsorption of cationic surfactant on silica at equilibrium. *J. Phys. Chem. B* **2001**, *105*, 1389-1402.

82 - Kékicheff, P.; Contal, C. Cationic surfactant-coated mica surfaces below the critical micellar concentration: 1 – Patchy structures as revealed by Peak Force Tapping AFM mode. *Langmuir* **2019**, *35* (8), 3087-3107.

83 - Ninham, B. W.; Parsegian, V. A. Electrostatic potential between surface bearing ionizable groups in ionic equilibrium with physiologic saline solution. *J. Theor. Biol.* **1971**, *31*, 405-428.

84 - Derjaguin, B. V. Theorie des Anhaftens kleiner Teilchen. *Kolloid Z.* **1934**, *69*, 155-164.

85 - Dzyaloshinskii, I. E.; Lifshitz, E. M.; Pitaevskii, L. P. The general theory of van der Waals forces. *Adv. Phys.* **1961**, *10*, 165-209.

86 - Eriksson, J. C.; Ljunggren, S.; Claesson, P. M. A phenomenological theory of long-range hydrophobic attraction forces based on a square-gradient variational approach. *J. Chem. Soc., Faraday Trans. 2* **1989**, *85*, 163-176.

87 - Attard, P. Long-range attraction between hydrophobic surfaces. *J. Phys. Chem.* **1989**, *93*, 6441-6444.

88 - Podgornik, R. Forces between surfaces with surface-specific interactions in a dilute electrolyte. *Chem. Phys. Lett.* **1989**, *156*, 71-75.

89 - Podgornik, R. Electrostatic correlation forces between surfaces with surface specific

ionic interactions. *J. Chem. Phys.* **1989**, *91*, 5840-5849.

90 - Tsao, Y.-H.; Evans, D. F., Wennerström, H. Long-range attraction between a hydrophobic surface and a polar surface is stronger than that between two hydrophobic surfaces. *Langmuir* **1993**, *97*, 779-785.

91 - Bérard, D. R.; Attard, P.; Patey, G. N. Cavitation of a Lennard-Jones fluid between hard walls, and the possible relevance to the attraction measured between hydrophobic surfaces. *J. Chem. Phys*. **1993**, *98*, 7236-7244.

92 - Yaminsky, V. V.; Ninham, B. W. Hydrophobic force: Lateral enhancement of subcritical fluctuations. *Langmuir* **1993**, *9*, 3618-3624.

93 - Spalla, O.; Belloni, L. Long range electrostatic attraction between neutral surfaces. *Phys. Rev. Lett.* **1995**, *74*, 2515-2518.

94 - Kékicheff, P.; Spalla, O. Long-range Electrostatic Attraction between Similar, Charge-neutral Walls. *Phys. Rev. Lett.* **1995**, *75*, 1851-1854.

95 - Belloni, L.; Spalla, O. Attraction of electrostatic origin between colloids. *J. Chem. Phys.* **1997**, *107*, 465-480.

96 - Boinovich, L. B. & Emelyanenko, A. M. On the theory of the phonon component of disjoining pressure of thin liquid films. *Zeitschrift für Physikalische Chemie.* **1992**, *178*, 229-241.

97 - Boinovich, L. B. & Emelyanenko, A. M. Forces due to dynamic structure in thin liquid films. *Adv. Colloid Interface Sci.* **2002**, *96*, 37-58.

98 - Kékicheff, P.; Iss, J.; Fontaine, P.; Johner, A. Direct Measurement of Lateral Correlations under Controlled Nanoconfinement. *Phys. Rev. Lett.* **2018**, *120* (11), 118001.

99 - Israelachvili, J. N.; Adams, G. E. Measurement of forces between two mica surfaces in aqueous electrolyte solutions in the range 0-100 nm. *J. Chem. Soc. Faraday Trans. 1* **1978**, *74*, 975-1001.

100 - Israelachvili, J. N. Thin Film Studies Using Multiple-Beam Interferometry. *J. Colloid Interface Sci.* **1973**, *44*, 259-272.

101 - Kékicheff, P.; Spalla, O. Refractive index of thin aqueous films confined between two hydrophobic surfaces. *Langmuir* **1994**, *10*, 1584-1591.

102 - Kékicheff, P. From heterocoagulation to biorecognition: Preparation of surfaces for direct measurement of their interactions in a Surface Force Apparatus. *Macromol. Symp.* **2014**, *335*, 24-42.

103 - Attard, P.; Parker, J. L. Deformation and adhesion of elastic bodies in contact. *Phys. Rev. A* **1992**, *46*, 7959-7971.

104 - Parker, J. L.; Attard, P. Deformation of surfaces due to surface forces. *J. Phys. Chem.* **1992**, *26*, 10398-10405.

105 - Israelachvili, J. N.; Tabor, D. The measurement of van der Waals dispersion forces in the range 1.5 to 130 nm. *Proc. R. Soc. Lond. A* **1972**, *331*, 19-38.

106 - Israelachvili, J. N.; Pashley, R. M. Measurement of the hydrophobic interaction between two hydrophobic surfaces in aqueous electrolyte solutions. *J. Colloid Interface Sci.* **1984**, *98*, 500-514.

107 - Rabinovich, Y. I. Direct measurements of the disjoining pressure in electrolyte solutions as a function of the distance between crossed filaments (in Russian). *Kolloidn. Zh.* **1977**, *39*, 1094-1100.

108 - Derjaguin, B. V.; Rabinovich, Y. I.; Churaev, N. V. Direct measurement of molecular forces. *Nature* **1978**, *272*, 313-318.

109 - Rabinovich, Y. I.; Derjaguin, B. V., in *Surface Forces and Boundary Liquid Layers*, edited by B. V. Derjaguin, Nauka, Moscow, 1983, p.13.

110 - Chan, D. Y. C.; Horn, R. G. The drainage of thin liquid films between solid surfaces. *J. Chem. Phys.* **1985**, *83*, 5311-5324.

111 - Vinogradova, O. Slippage of water over hydrophobic surfaces. *Int. J. Miner. Process.* **1999**, *56*, 31-60.

112 - Cottin-Bizonne, C.; Jurine, S.; Baudry, J.; Crassous, J.; Restagno, F.; Charlaix, É. Nanorheology: An investigation of the boundary condition at hydrophobic and hydrophilic interfaces. *Eur. Phys. J. E* **2002**, *9*, 47-53.

113 - Ducker, W. A.; Senden, T. J.; Pashley, R. M. Direct measurement of colloidal forces using an atomic force microscope. *Nature* **1991**, *353*, 239-241.

114 - Butt, H.-J. Measuring electrostatic, van der Waals, and hydration forces in electrolyte solutions with an atomic force microscope. *Biophysical J.* **1991**, ***60***, 1438-1444.

115 - Butt, H.-J. ; Capella, B.; Kappl, M. Force measurements with the atomic force microscope: Technique, interpretation and applications. *Surf. Sci. Rep.* **2005**, *59*, 1-152.

116 - Borkovec, M.; Szilagyi, I.; Popa, I.; Finessi, M.; Sinha, P.; Maroni, P.; Papastavrou, G. Investigating forces between charged particles in the presence of oppositely charged polyelectrolytes with the multi-particle colloidal probe technique. *Adv. Colloid Interface Sci.* **2012**, *179-182*, 85–98.

117 - Parker, J. L. A new method for measuring the force between two surfaces in a Surface Force Apparatus. *Langmuir* **1992**, *8*, 551-556.

118 - Parker, J. L. Surface force measurements in surfactant systems. *Progr. Surface Sci.* **1994**, *47*, 205-271.

119 - Christenson, H. K. Adhesion between surfaces in undersaturated vapors — A reexamination of the influence of meniscus curvature and surface forces. *J. Colloid Interface Sci.* **1988**, *121*, 170-178.

120 - Sharma, B. G.; Basu, S.; Sharma, M. M. Characterization of adsorbed ionic surfactants on a mica substrate, *Langmuir* **1996**, *12*, 6506-6512.

121 - Teschke, O.; Ceotto, G.; de Souza, E. F. Imaging of soft structures: dependence of contrast in atomic force microscopy images on the force applied by the tip. *J. Vac. Sci. Technol. B* **2000**, *18*, 1144-1150.

122 - Fleming, B. D.; Biggs, S.; Wanless, E. J. Slow organization of cationic surfactant adsorbed to silica from solutions far below the CMC. *J. Phys. Chem. B* **2001**, *105*, 9537-9540.

123 - Fujii, M.; Li, B.; Fukada, K.; Kato, T.; Seimiya, T. Two-dimensional arrangements of adsorbed alkylammonium halides on cleaved mica surface. *Langmuir* **2001**, *17*, 1138-1142.

124 - Cao, M.; Wang, X.-L. Direct observation and distinction of the inner/outer layers of surfactant bilayer formed at the solid/solution Interface. *J. Dispers. Sci. Technol.* **2010**, *31*, 38-43.

125 - Zorin, Z. M.; Churaev, N. V.; Esipova, N. E.; Sergeeva, I. P.; Sobolev, V. D.; Gasanov, E. K. Influence of cationic surfactant on the surface charge of silica and on the stability of aqueous wetting films. *J. Colloid Interface Sci.* **1992**, *152*, 170-182.

126 - Churaev, N .V.; Sergeeva I. P.; Sobolev, V. D.; Jacobasch, H.-J.; Weidenhammer, P.; Schmitt, F.-J. Modification of quartz surfaces using cationic surfactant solutions. *Colloids Surf. A* **2000**, *164*, 121-129.

127 - Grosse, I.; Estel, K. Thin surfactant layers at the solid interface. *Colloid Polym. Sci.* **2000**, *278*, 1000-1006.

128 - Theodoly, O.; Cascao-Pereira, L.; Bergeron, V.; Radke, C. J. A combined streaming-potential optical reflectometer for studying adsorption at the water/solid interface. *Langmuir* **2005**, *21*, 10127-10139.

129 - Rennie, A. R.; Lee, E. M.; Simister, E. A.; Thomas, R. K. Structure of a cationic surfactant layer at the silica-water interface. *Langmuir* **1990**, *6*, 1031-1034.

130 - McDermott, D. C.; McCarney, J.; Thomas, R. K.; Rennie, A. R. Study of an adsorbed layer of hexadecyltrimethylammonium bromide using the technique of neutron reflection. *J. Colloid Interface Sci.* **1994**, *162*, 304–310.

131 - Fragneto, G.; Thomas, R. K.; Rennie, A. R.; Penfold, J. Neutron reflection from hexadecyltrimethylammonium bromide adsorbed on smooth and rough silicon surfaces. *Langmuir* **1996**, *12*, 6036–6043.

132 - Penfold, J.; Staples, E. J.; Tucker, I.; Thompson, L. J. Adsorption of mixed cationic and non ionic surfactants at the hydrophilic silicon surface from aqueous solution: Studied by specular neutron reflection. *Langmuir* **1997**, *13*, 6638-6643.

133 - Penfold, J.; Tucker, I.; Petkov, J.; Thomas, R. K. Surfactant adsorption onto cellulose surfaces. *Langmuir* **2007**, *23*, 8357–8364.

134 - Briscoe, W. H.; Speranza, F.; Li, P.; Konovalov, O.; Bouchenoire, L.; van Stam, J.; Klein, J.; Jacobs, R. M. J.; Thomas, R. K. Synchrotron XRR study of soft nanofilms at the mica-water interface. *Soft Matter* **2012**, *8*, 5055-5068.

135 - Speranza, F.; Pilkington, G. A.; Dane, T. G.; Cresswell, P. T.; Li, P.; Jacobs, R. M. J.; Arnold, T.; Bouchenoire, L.; Thomas, R. K.; Briscoe, W. H. Quiescent bilayers at the mica-water interface. *Soft Matter* **2013**, *9*, 7028-7041.

136 - Pagac, E. S.; Prieve, D. C.; Tilton, R. D. Kinetics and mechanism of cationic surfactant adsorption and coadsorption with cationic polyelectrolytes at the silica-water interface. *Langmuir* **1998**, *14*, 2333-2342.

137 - Atkin, R.; Craig, V. S. J.; Biggs, S. Adsorption kinetics and structural arrangements of cationic surfactants on silica surfaces. *Langmuir* **2000**, *16*, 9374-9380.

138 - Howard, S. C.; Craig, V. S. J. Very slow surfactant adsorption at the solid-liquid interface is due to long lived surface aggregates. *Soft Matter* **2009,** *5,* 3061-3069.

139 - Chen, Y. L.; Chen, S.; Frank, C.; Israelachvili, J. Molecular mechanisms and kinetics during the self-assembly of surfactant layers. *J. Colloid Interface Sci.* **1992**, *153*, 244-265

140 - Li, B.; Fujii, M.; Fukada, K.; Kato, T.; Seimiya, T. Time dependent anchoring of adsorbed cationic surfactant molecules at mica/solution interface, *J. Colloid Interface Sci.* **1999**, *209*, 25-30.

141 - Kung, K.-H. S.; Hayes, K. F. Fourier-Transform infrared spectroscopic study of the adsorption of cetyltrimethylammonium bromide and cetylpyridinium chloride on silica. *Langmuir* **1993**, *9*, 263-267.

142 - Neivandt, D. J.; Gee, M. L.; Tripp, C. P.; Hair, M. L. Coadsorption of poly(styrenesulfonate) and cetyltrimethylammonium bromide on silica investigated by Attenuated Total Reflection techniques. *Langmuir* **1997**, *13*, 2519-2526.

143 - Neivandt, D. J.; Gee, M. L.; Hair, M. L.; Tripp, C. P. Polarized Infrared Attenuated Total Reflection for the in situ determination of the orientation of surfactant adsorbed at the solid/solution interface. *J. Phys. Chem. B* **1998**, *102*, 5107-5114.

144 - Wang, W.; Gu, B.; Liang, L.; Hamilton, W. A. Adsorption and structural arrangement of cetyltrimethylammonium cations at the silica nanoparticle-water interface. *J. Phys. Chem.* **2004**, *108*, 17477-17483.

145 - Ström, C.; Hansson, P.; Jönsson, B.; Söderman, O. Size of cationic surfactant micelles at the silica-water interface: A fluorescent probe study. *Langmuir* **2000**, *16*, 2469-2474.

146 - Tyrode, E.; Rutland, M. W.; Bain, C. D. Adsorption of CTAB on hydrophilic silica studied by linear and nonlinear optical spectroscopy. *J. Am. Chem. Soc.* **2008**, *130*, 17434-

17445.

147 - Woods, D. A.; Petkov, J.; Bain, C. D. Surfactant adsorption kinetics by Total Internal Reflection Raman spectroscopy. 1. Pure surfactants on silica. *J. Phys. Chem. B* **2011**, *115*, 7341-7352

148 - Schönhoff, M. NMR methods for studies of organic adsorption layers. In: Möbius D, Miller R, editors. Novel methods to study interfacial layers. Amsterdam: Elsevier; 2001. p. 285–336.

149 - Schönhoff, M. NMR studies of sorption and adsorption phenomena in colloidal systems. *Curr. Opin. Colloid Interface Sci.* **2013**, *18*, 201-213.

150 - Söderlind, E.; Stilbs, P. Chain conformation of ionic surfactants adsorbed on solid surfaces from ^{13}C NMR chemical shifts. *Langmuir* **1993**, *9*, 1678-1683.

151 - Biswas, S. C. & Chattoraj, D. K. Kinetics of adsorption of cationic surfactants at silica-water interface. *J. Colloid Interface Sci.* **1998**, *205*, 12-20.

152 - Johnson, R. A.; Nagarajan, R. Modeling self-assembly of surfactants at solid liquid interfaces. II. Hydrophilic surfaces. *Colloids Surf. A: Physicochem. Eng. Aspects* **2000**, 167, 21-30.

153 - Klebow, B.; Meleshyn, A. Aggregation of alkytrimethylammonium ions at the cleaved muscovite mica-water interface: A Monte Carlo study. *Langmuir* **2011**, *27*, 12968-12976.

154 - Jiménez-Angeles, F.; Khoshnood, A.; Firoozabadi, A. Molecular dynamics simulation of the adsorption and aggregation of ionic surfactants at liquid-solid interfaces. *J. Phys. Chem. C* **2017**, *121*, 25908-25920.

155 - Pashley, R. M.; Israelachvili, J. N. A comparison of surface forces and interfacial properties of mica in purified surfactant solutions. *Colloids Surf.* **1981**, *2*, 169-187.

156 - Craig, V. S. J.; Ninham, B. W.; Pashley, R. M. Study of the long-range hydrophobic attraction in concentrated salt solutions and its implications for electrostatic models. *Langmuir* **1998**, *14*, 3226-3232.

157 - Lüderitz, L. A. C.; von Klitzing, R. Interaction forces between silica surfaces in cationic surfactant solutions: An atomic force microscopy study. *J. Colloid Interface Sci.* **2013**, *402*, 19-26.

158 - Iler, R. K. *The chemistry of silica.* Wiley: New York, 1979.

159 - Atkins, D.; Kékicheff, P.; Spalla, O. Adhesion between colloidal silica as seen with direct force measurement. *J. Colloid Interface Sci.* **1997**, *188*, 234-237.

160 - Fontaine, P.; Ciatto, G.; Aubert, N.; Goldmann, M. Soft interfaces and resonant investigation on undulator source: A surface X-ray scattering beamline to study organic molecular films at the SOLEIL synchrotron. *Sci. Adv. Mater.* **2014**, *6*, 2312-2316.

161 - Idziak, S. H. J.; Safinya, C. R.; Hill, R. S.; Kraiser, K. E.; Ruths, M.; Warriner, H. E.; Steinberg, S.; Liang, K. S.; Israelachvili, J. N. The X-ray surface forces apparatus: Structure of a thin smectic liquid crystal under confinement. *Science* **1994**, *264*, 1915-1918.

162 - Golan, Y.; Martin-Herranz, A.; Li, Y.; Safinya, C. R.; Israelachvili, J. Direct observation of shear-induced orientational phase coexistence in a lyotropic system using a modified x-ray Surface Forces Apparatus. *Phys. Rev. Lett.* **2001**, *86*, 1263-1266.

163 - Zana, R.; Yiv, S.; Strazielle, C.; Lianos, P. Effect of alcohol on the properties of micellar systems. I. Critical micellization concentration, micelle molecular weight and ionization degree, and solubility of alcohols in micellar solutions. *J. Colloid Interface Sci.* **1981**, *80*, 208-223.

164 - Van Os, N. M.; Haak, J. R.; Haak, L. A. M. *Physicochemical Properties of Selected Anionic, Cationic, and Nonionic Surfactants*; Elsevier: New York, 1993.

165 - Lifshitz, E. M. The theory of molecular attractive forces between solids. *J. Exper. Theoret. Phys. USSR* **1955**, *29*, 94-110 (*Sov. Phys. JETP* **1956**, *2*, 73-83).

166 - Ninham, B. W.; Parsegian, V. A. Van der Waals forces, Special characteristics in lipid-water systems and a general method of calculation based on the Lifshitz theory. *Biophys. J.* **1970**, *10*, 646-663.

167 - Parsegian, V. A. *Van der Waals Forces: A Handbook for Biologists, Chemists, Engineers, and Physicists*, Cambridge Univ. Press, New York, 380 pp. (2006).

168 - Claesson, P. M.; Blom, C. E.; Herder, P. C.; Ninham, B. W. Interactions between water-stable hydrophobic Langmuir-Blodgett monolayers on mica. *J. Colloid Interface Sci.* **1986**, *114*, 234-242.

169 - Christenson, H. K.; Claesson, P. M. Cavitation and the interaction between macroscopic hydrophobic surfaces. *Science* **1988**, *239*, 390-392.

170 - Claesson, P.M.; Christenson, H. K. Very long range attractive forces between uncharged hydrocarbon and fluorocarbon surfaces in water. *J. Phys. Chem.* **1988**, *92*, 1650-1655.

171 - Herder, P. C. Forces between hydrophobed mica surfaces immersed in dodecylammonium chloride solutions. *J. Colloid Interface Sci.* **1990**, *134*, 336-345.

172 - Christenson, H. K.; Fang, J.; Ninham, B. W.; Parker, J. L. Effect of divalent electrolyte on the hydrophobic attraction. *J. Phys. Chem.* **1990**, *94*, 8004-8006.

173 - Wood, J.; Sharma, R. Interaction forces between hydrophobic mica surfaces. *J. Adhesion Sci. Technol.* **1995**, *9*, 1075-1085.

174 - Hato, M. Attractive forces between surfaces of controlled “hydrophobicity” across water: A possible range of “hydrophobic interactions” between macroscopic hydrophobic surfaces across water. *J. Phys. Chem.* **1996**, *100*, 18530-18538.

175 - Eriksson, L. G. T.; Claesson, P. M.; Ohnishi, S.; Hato, M. Stability of dimethyldioctadecylammonium bromide Langmuir-Blodgett films on mica in aqueous salt solutions — implications for surface force measurements. *Thin Solid Films* **1997**, *300*, 240-255.

176 - Lin, Q.; Meyer, E. E.; Tadmor, M.; Israelachvili, J. N.; Kuhl, T. L. Measurement of the long- and short-range hydrophobic attraction between surfactant-coated surfaces. *Langmuir* **2005**, *21*, 251-255.

177 - Meyer, E. E.; Lin, Q.; Israelachvili, J. N. Effect of dissolved gas on the hydrophobic attraction between surfactant-coated surfaces. *Langmuir* **2005**, *21*, 256-259.

178 - Herder, P. C.; Claesson, P. M.; Herder, C. E. Adsorption of cationic surfactants on muscovite mica as quantified by means of ESCA. *J. Colloid Interface Sci.* **1987**, *119*,155-167.

179 - Hähner, G.; Zwahlen, M.; Caseri, W. Chain-length dependence of the conformational order in self-assembled dialkylammonium monolayers on mica studied with soft x-ray absorption. *Langmuir* **2005**, *21*, 1424-1427.

180 - Osman M. A.; Ernst, M.; Meier, B. H.; Suter, U. W. Structure and molecular dynamics of alkane monolayers self-assembled on mica platelets. *J. Phys. Chem. B* **2002**, *106*, 653-662.

181 - Tsao, Y.-H.; Yang, S. X.; Evans, D. F.; Wennerström, H. Interactions between hydrophobic surfaces. Dependence on Temperature and alkyl chain length. *Langmuir* **1991**, *7*, 3154-3159.

182 - Rabinovich, Ya. I.; Guzonas, D. A.; Yoon, R.-H. Role of chain order in the long-range attractive force between hydrophobic surfaces. *Langmuir* **1993**, *9*, 1168-1170.

183 - Kékicheff, P., Marcelja, S., Senden, T. J., Shubin, V. E. Charge reversal seen in electrical double layer interaction of surfaces immersed in 2:1 calcium electrolyte. *J. Chem. Phys.* **1993**, *99*, 6098-6113.

184 - Kielland, J. Individual activity coefficients of ions in aqueous solutions. *J. Am. Chem. Soc.* **1937**, *59*, 1675-1678

185 - Robinson, R. A.; Stokes, R. H. *Electrolyte Solutions*, 2nd ed.; Academic Press: New York, 1961; Chapter 9.

186 - Murray, J. W. Activity scales and activity corrections (chapter 6), in: *Chemical Oceanography*, Oxford Press, in progress, 2019.

187 - Davies, C. W. Incomplete dissociation in aqueous salt solutions, in Hamer, W. J., ed. *Structure of electrolytic solutions*: New York, John Wiley and Sons, Inc. p. 26-29, 1959.

188 - Bigelow, W. C.; Pickett, D. L.; Zisman, W. A. Oleophobic monolayers. 1. Films adsorbed from solution in non-polar liquids. J. *Colloid Sci.* **1946**, *1* (6), 513−538.

189 - Cecil, R. Model system for hydrophobic interactions. *Nature* **1967**, *214*, 369-370.

190 - Sagiv, J. Organized monolayers by adsorption. 1. Formation and structure of oleophobic mixed monolayers on solid surfaces. *J. Am. Chem. Soc.* **1980**, 102, 92-98.

191 - Maoz, R.; Sagiv, J. On the formation and structure of self-assembling monolayers. I. A comparative ATR-wettability study of Langmuir-Blodgett and adsorbed films on flat substrates and glass microbeads. *J. Colloid Interface Sci.* **1984**, *100*, 465-496.

192 - Tripp, C. P.; Hair, M. L. Reaction of chloromethylsilanes with silica: A low-frequency infrared study. *Langmuir* **1991**, *7*, 923-927.

193 - Tripp, C. P.; Hair, M. L. Chemical attachment of chlorosilanes to silica: A two-step amine-promoted reaction. *Langmuir* **1993**, *97*, 5693-5698.

194 - Tripp, C. P.; Hair, M. L. Reaction of methylsilanols with hydrated silica surfaces: The hydrolysis of trichloro-, dichloro-, and monochloromethylsilanes and the effects of curing. *Langmuir* **1995**, *11*, 149-155.

195 - Combes, J. R.; White, L. D.; Tripp, C. P. Chemical modification of metal oxide surfaces in supercritical CO_2: In situ infrared studies of the adsorption and reaction of organosilanes on silica. *Langmuir* **1999**, *15*, 7870-7875.

196 - Wang, Y.; Lieberman, M. Growth of ultrasmooth octadecyltrichlorosilane self-assembled monolayers on SiO_2. *Langmuir* **2003**, *19*, 1159-1167.

197 - Bernardoni, F.; Kouba, M.; Fadeev, A. Y. Effect of curvature on the packing and ordering of organosilane monolayers supported on solids. *Chem. Mater.* **2008**, *20*, 382-387.

198 - Li, Z.; Yoon, R.-H. Thermodynamics of hydrophobic interaction between silica surfaces coated with octadecyltrichlorosilane. *J. Colloid Interface Sci.* **2013**, *392*, 369-375.

199 - Lessel, M.; Bäumchen, O.; Klos, M.; Hähl, H.; Fetzer, R.; Paulus, M.; Seemann, R. Self-assembled silane monolayers: An efficient step-by-step recipe for high-quality, low-energy surfaces. *Surf. Interface Anal.* **2015**, *47*, 557-564.

200 - Silberzan, P.; Léger, L.; Ausserré, D.; Benattar, J. J. Silanation of silica surfaces. A new method of constructing pure or mixed monolayers. *Langmuir* **1991**, *7*, 1647-1651.

201 - Barrat, A.; Silberzan, P.; Bourdieu, L.; Chatenay, D. How are the wetting properties of silanated surfaces affected by their structure? An Atomic Force Microscopy study. *Europhys. Lett.* **1992**, *20*, 633-638.

202 - Brzoska, J. B.; Ben Azouz, I.; Rondelez, F. Silanization of solid substrates: A step toward reproducibility. *Langmuir* **1994**, *10*, 4367-4373.

203 - Geer, R. E.; Stenger, D. A.; Chen, M. S.; Calvert, J. M.; Shashidhar, R.; Jeong, Y. H.; Pershan, P. S. X-ray and ellipsometric studies of self-assembled monolayers of fluorinated chlorosilanes. *Langmuir* **1994**, *10*, 1171-1176.

204 - Bourdieu, L.; Daillant, J.; Chatenay, D.; Braslau, A.; Colson, D. Buckling of polymerized monomolecular films. *Phys. Rev. Lett.* **1994**, *72*, 1502-1505.

205 - Murphy, M. A.; Nordgren, C. E.; Fischetti, R. F.; Blasie, J. K.; Peticolas, L. J.; Bean, J. C. Structural study of the annealing of alkylsiloxane self-assembled monolayers on silicon by high-resolution X-ray diffraction. *J. Phys. Chem.* **1995**, *99*, 14039-14051.

206 - Davidovits, J. V.; Pho, V.; Silberzan, P.; Goldmann, M. Temperature influence on the formation of silanized monolayers on silica: An atomic force microscopy study. *Surf. Sci.* **1996**, *352-354*, 369-373.

207 - Goldmann, M.; Davidovits, J. V.; Silberzan, P. Kinetics of self-assembled silane monolayers at various temperatures: evidence of 2D foam. *Thin Solid Films* **1998**, *327-329*, 166-171.

208 - Vallant, T.; Brunner, H.; Mayer, U.; Hoffmann, H.; Leitner, T.; Resch, R.; Friedbacher, G. Formation of self-assembled octadecylsiloxane monolayers on mica and silicon surfaces studied by atomic force microscopy and infrared spectroscopy. *J. Phys. Chem. B* **1998**, *102*, 7190-7197.

209 - Fadeev, A. Y.; McCarthy, T. J. Trialkylsilane monolayers covalently attached to silicon surfaces: Wettability studies indicating that molecular topography contributes to contact angle hysteresis. *Langmuir* **1999**, *15*, 3759-3766.

210 - Wang, M.; Liechti, K. M.; Wang, Q.; White, J. M. Self-assembled silane monolayers: Fabrication with nanoscale uniformity. *Langmuir* **2005**, *21*, 1848-1857.

211 - Jalali, H.; Gates, B. D. Monitoring and mapping imperfections in silane-based self-assembled monolayers by chemical amplification. *Langmuir* **2009**, *25*, 9078-9084.

212 - Van Ooij, W. J.; Zhu, D.; Palanivel, V. Lamar, A.; Stacy, M. Overview: The Potential of silanes for chromate replacement in metal finishing industries. *Silicon Chemistry* **2006**, *3*, 11-30.

213 - Carson, G. A.; Granick, S. Self-assembly of octadecyltrichlorosilane monolayers on mica. *J. Mater. Res.* **1980**, *5*, 1745-1751.

214 - Guzonas, D. A.; Hair, M. L.; Tripp, C. P. Infrared spectra of monolayers adsorbed on mica. *Appl. Spectrosc.* **1990**, *44*, 290-293.

215 - Schwartz, D. K.; Steinberg, S. S.; Israelachvili, J.; Zasadzinski, J. A. N. Growth of a self-assembled monolayer by fractal aggregation. *Phys. Rev. Lett.* **1992**, *69*, 3354-3357.

216 - Wood, J.; Sharma, R. Preparation of a robust hydrophobic monolayer on mica. *Langmuir* **1994**, *10*, 2307-2310.

217 - Nakagawa, T.; Ogawa, K.; Kurumizawa, T. Atomic force microscope images of monolayers from alkyltrichlorosilane on mica surfaces and studies on an anchoring mechanism of alkyltrichlorosilane molecules to the surface. *Langmuir* **1994**, *10*, 525-529.

218 - Peanasky, J.; Schneider, H. M.; Granick, S.; Kessel, C. R. Self-assembled monolayers on mica for experiments utilizing the Surface Forces Apparatus. *Langmuir* **1995**, *11*, 953-962.

219 - Xiao, X.-D.; Liu, G.-Y.; Charych, D. H.; Salmeron, M. Preparation, structure, and mechanical stability of alkylsilane monolayers on mica. *Langmuir* **1995**, *11*, 1600-1604.

220 - Britt, D. W.; Hlady, V. An AFM study of the effects of silanization temperature, hydration, and annealing on the nucleation and aggregation of condensed OTS domains on mica. *J. Colloid Interface Sci.* **1996**, *178*, 775-784.

221 - Nakagawa, T.; Soga, M. Contact angle and atomic force microscopy study of reactions of *n*-alkyltrichlorosilanes with muscovite micas exposed to water vapor plasmas with various power densities. *Jpn. J. Appl. Phys.* **1997**, *36*, 6915-6921.

222 - Barrena, E.; Kopta, S.; Ogletree, D. F.; Charych, D. H.; Salmeron, M. Relationship between friction and molecular structure: Alkylsilane lubricant films under pressure. *Phys. Rev. Lett.* **1999**, *82*, 2880-2883.

223 - Lambert, A. G.; Neivandt, D. J.; McAloney, R. A.; Davies, P. B. A protocol for the reproducible silanization of mica validated by Sum Frequency Spectroscopy and Atomic Force Microscopy. *Langmuir* **2000**, *16*, 8377-8382.

224 - Doudevski, I.; Hayes, W. A.; Woodward, J. T.; Schwartz, D. K. Atomic force microscope imaging of molecular aggregation during self-assembled monolayer growth. *Colloids Surf. A* **2000**, *174*, 233-243.

225 - Kim, S.; Christenson, H. K.; Curry, J. E. The effect of humidity on the stability of an octadecyltriethoxysilane monolayer self-assembled on untreated and plasma-treated mica. *Langmuir* **2002**, *18*, 2125-2129.

226 - Malham, I. B.; Bureau, L. Growth and stability of a self-assembled monolayer on plasma-treated mica. *Langmuir* **2009**, *25*, 5631-5636.

227 - Benitez, J. J.; Heredia-Guerrero, J. A.; San-Miguel, M. A.; Gallloway, H. C. Packing defects in fatty amine self-assembled monolayers on mica as revealed from AFM techniques. *J. Phys. Chem. B* **2018**, *122*, 493-499.

228 - Flinn, D. H.; Guzonas, D. A.; Yoon, R.-H. Characterization of silica surfaces hydrophobized by octadecyltrichlorosilane. *Colloids Surf. A* **1994**, *87*, 163-176.

229 - Kim, S.; Christenson, H. K.; Curry, J. E. The effect of humidity on the stability of an octadecyltriethoxysilane monolayer self-assembled on untreated and plasma-treated mica. *Langmuir* **2002**, *18*, 2125-2129.

230 - Blake, P.; Ralston, J. Controlled methylation of quartz particles. *Colloids Surf.* **1985**, 15, 101-118.

231 – Mahanty, J.; Ninham, B. W. *Dispersion Forces*, Academic Press, London, New York, San Francisco, 1976.

232 - Lee, C.-Y.; McCammon, J. A.; Rossky, P. J. The structure of liquid water at an extended hydrophobic surface. *J. Chem. Phys.* **1984**, *80*, 4448-4455.

233 - Kjellander, R.; Marcelja, S. Polarization of water between molecular-surfaces A molecular dynamics study. *Chem. Scr.* **1985**, *25*, 73-80.

234 - Luzar, A.; Bratko, D.; Blum, L. Monte Carlo simulation of hydrophobic interaction. *J. Chem. Phys.* **1987**, *86*, 2955-2959.

235 - Valleau, J. P.; Gardner A. A. Water-like particles at surfaces. I. The uncharged, unpolarizable surface. *J. Chem. Phys.* **1987**, *86*, 4162-4170.

236 - Evans, R.; Marini Bettolo Marconi, U. Phase equilibria and solvation forces for fluids confined between parallel walls. *J. Chem. Phys.* **1987**, *86*, 7138-7148.

237 - Lum, K; Chandler, D.; Weeks, J. D. Hydrophobicity at small and large length scales. *J. Phys. Chem. B* **1999**, *103*, 4570-4577.

238 - Bratko, D.; Curtis, R. A.; Blanch, H. W.; Prausnitz, J. M. Interaction between hydrophobic surfaces with metastable intervening liquid. *J. Chem. Phys.* **2001**, *115*, 3873-3877.

239 - Mamatkulov, S. I.; Khabibullaev, P. K.; Netz, R. R. Water at hydrophobic substrates: curvature, pressure, and temperature effects. *Langmuir* **2004**, 20, 4756-4763.0

240 - Schwendel, D.; Hayashi, T.; Dahint, R.; Pertsin, A.; Grunze M.; Steitz, R.; Schreiber, F. Interaction of water with self-assembled monolayers: Neutron reflectivity measurements of he water density in the interface region. *Langmuir* **1003**, *19*, 2284-2293.

241 - Doshi, D. A.; Watkins, E. B.; Israelachvili, J. N.; Majewski, J. Reduced water density at hydrophobic surfaces: Effect of dissolved gases. *Proc. Natl. Acad. Sci. USA* **2005**, *102*, 9458-9462.

242 - Seo, Y.-S.; Satija, S. No intrinsic depletion layer on a polystyrene thin film at a water interface. *Langmuir* **2006**, *22*, 7113-7116.

243 - Gutfreund, P.; Maccarini, M.; Dennison, A. J. C.; Wolff, M. The search for nanobubbles by using specular and off-specular neutron reflectometry. *Langmuir* **2016**, *32*, 9091-9096.

244 - Mezger, M.; Reichert, H.; Schöder, S.; Okasinski, J.; Schröder, H.; Dosch, H.; Palms, D.; Ralston, J.; Honkimäki, V. High-resolution *in situ* x-ray study of the hydrophobic gap at the water-octadecyl-trichlorosilane interface. *Proc. Natl. Acad. Sci. U.S.A.* **2006**, *103*, 18401-18404.

245 - Mezger, M.; Sedlmeier, F.; Horinek, D.; Reichert, H.; Pontoni, D.; Dosch, H. On the origin of the hydrophobic water gap: An x-ray reflectivity and MD simulation study. *J. Am. Chem. Soc.* **2010**, 132, 6735-6741.

246 - Christenson, H. K.; Yaminsky, V. V. Is the long-range hydrophobic attraction related to the mobility of hydrophobic surface groups? *Colloids Surf. A* **1997**, *129-130*, 67-74.

247 - Miklavic, S. J.; Chan, D. Y.C.; White, L. R.; Healy, T. W. Double layer forces between heterogeneous charged surfaces. *J. Phys. Chem.* **1994**, *98*, 9022-9030.

248 - Perkin, S.; Kampf, N.; and Klein, J. Long-ranged attraction between charge-mosaic surfaces across water. *Phys. Rev. Lett.* **2006**, *96*, 038301.

249 - Perkin, S.; Kampf, N.; Klein, J. Stability of self-assembled hydrophobic surfactant layers in water. *J. Phys. Chem.* **2005**, *109*, 3832-3837.

250 - Silbert, G.; Ben-Yaakov, D.; Dror, Y.; Perkin, S.; Kampf, N.; Klein, J. Long-ranged attraction between disordered heterogeneous surfaces. *Phys. Rev. Lett.* **2012**, *109*, 168305.

251 - Naji, A.; Podgornik, R. Quenched charge disorder and Coulomb interactions. *Phys. Rev. E* **2005**, *72*, 041402.

252 - Bakhshandeh, A.; dos Santos, A. P.; Diehl, A., Levin, Y. Interaction between random heterogeneously charged surfaces in an electrolyte solution. *J. Chem. Phys.* **2015**, *142*, 194707.

253 - Donaldson, S. H.; Royne, A.; Kristiansen, K.; Rapp, M. V.; Das, S.; Gebbie, M. A.; Lee, D. W.; Stock, P.; Valtiner, V.; Israelachvili, J. N. Developing a general interaction potential for hydrophobic and hydrophilic interactions. *Langmuir* **2015**, *31*, 2051-2064.

254 - LeNeveu, D. M., Rand, R. P. & Parsegian, V. A. (1976). Measurements of forces between lecithin bilayers. *Nature (London)* **1976**, *259*, 601-603.

255 - LeNeveu, D. M., Rand, R. P., Parsegian, V. A., Gingell, D. Measurement and modification of forces between lecithin bilayers. *Biophys. J.* **1977**, *18*, 209-230.

256 - Pashley, R. M. DLVO and hydration forces between mica surfaces in Li^+, Na^+, K^+, and Cs^+ electrolyte-solutions: A correlation of double-layer and hydration forces with surface cation exchange properties. *J. Colloid Interface Sci.* **1981**, *83*, 531-546.

257 - Peschel, G., Belouschek, P., Müller, M. M., Müller, M. R., König, R. The interaction of solid surfaces in aqueous systems. Co*lloid Polym. Sci*. **1982**, *260*, 444-451.

258 - Rau, D. C.; Lee, B.; Parsegian, V. A. Measurement of the repulsive force between poly-electrolyte molecules in ionic solution - Hydration forces between parallel DNA double helices. *Proc. Natl. Acad. Sci. U.S.A.* **1984**, *81*, 2621-2625.

259 - Marra, J.; Israelachvili, J. Direct measurements of forces between phosphatidylcholine and phosphatidylethanolamine bilayers in aqueous electrolyte solutions. *Biochemistry* **1985**, *24*, 4608-4618.

260 - Rand, R. P.; Parsegian, V. A. Hydration forces between phospholipid-bilayers. *Biochim. Biophys. Acta* **1989**, *988*, 351-376.

261 - Grabbe, A.; Horn, R. G. Double-layer and hydration forces measured between silica sheets subjected to various surface treatments. *J. Colloid Interface Sci*. **1993**, *157*, 375-383.

262 - Loverde, S. M.; Velichko, Y. S.; de la Cruz, M. O. Competing interactions in two dimensional Coulomb systems: Surface charge heterogeneities in coassembled cationic-anionic incompatible mixtures. *J. Chem. Phys.* **2006**, *124*, 144702.

263 - Briscoe, W. H. Aqueous boundary lubrication: Molecular mechanisms, design strategy, and *terra incognita*. *Current opinion in Colloid Interface Sci*. **2017**, *27*, 1-8.

264 - Sakomoto, M.; Kanda, Y.; Miyahara, M.; Higashitani, K. Origin of long-range attractive force between surfaces hydrophobized by surfactant adsorption. *Langmuir* **2002**, *18*, 5713-5719.

265 - Zhang, J.; Yoon, R.-H.; Mao, M.; Ducker, W. A. Effects of degassing and ionic strength on AFM force measurements in octadecyltrimethylammonium chloride solutions. *Langmuir* **2005**, *21*, 5831-5841.

266 - Pashley, R. M.; Quirk, J. P. Ion exchange and interparticle forces between clay surface. *Soil Sci. Soc. Am. J.* **1989**, *53*, 1660-1667.

267 - Stevens, M. J. Thoughts on the structure of alkylsilane monolayers. *Langmuir* **1999**, *15*, 2773-2778.

268 - Attard, P.; Kjellander, R.; Mitchell, D. J.; Jönsson, B. Electrostatic fluctuation interactions between neutral surfaces with adsorbed, mobile ions or dipoles. *J. Chem. Phys.* **1988**, *89*, 1664-1680.

269 – Roger, K.; Cabane, B. Uncontaminated hydrophobic / water interfaces are uncharged: A reply. *Angew. Chem. Int. Ed.* **2012**, *51*, 12943-12945.